The Role of Charge-Matching in Nanoporous Materials Formation

Alessia Centi[1,¥], Joseph R. H. Manning[2], Vibha Srivastava[2], Sandra van Meurs[3], Siddharth V. Patwardhan[2,], Miguel Jorge[1,*]*

[1] Department of Chemical and Process Engineering, University of Strathclyde, 75 Montrose Street, Glasgow G1 1XJ, United Kingdom

[2] Department of Chemical and Biological Engineering, University of Sheffield, Mappin Street, Sheffield S13JD, United Kingdom

[3] Department of Chemistry, University of Sheffield, Brook Hill, Sheffield S3 7HF, United Kingdom

[*] Email: Miguel.jorge@strath.ac.uk; s.patwardhan@sheffield.ac.uk

[¥] Present address: Max Planck Institute for Polymer Research, Ackermannweg 10, 55128 Mainz, Germany

Abstract

Unravelling the molecular-level mechanisms that lead to the formation of mesoscale-ordered porous materials is a crucial step towards the goal of computational material design. For silica templated by alkylamine surfactants, a mechanism based on hydrogen-bond interactions between neutral amines and neutral silicates in solution has been widely accepted by the materials science community, despite the lack of conclusive evidence to support it. We demonstrate, through a combination of experimental measurements and multi-scale modelling, that the so-called "neutral templating route" does not represent a viable description of the synthesis mechanism of hexagonal mesoporous silica (HMS), the earliest example of amine-templated porous silica. Instead, the mesoscale structure of the material is defined by charge-matching of ionic interactions between amines and silicates. This has profound implications for the synthesis of a wide range of templated porous materials, and may shed new light on developing sustainable and economical routes to high value porous materials.

The discovery of templated periodic mesoporous silica (PMS) in the early 1990's, of which MCM-41 is the archetypal example [1], heralded a new era in material science research. This revolutionary approach, whereby the porous structure of the material is determined by co-operative self-assembly of silicates and surfactant molecules (originally cationic ammonium

compounds) in solution [2-4], allowed scientists to apply soft-matter physics principles to the synthesis of solid-state materials, enabling an unprecedented degree of control over the properties of the final material [5] and leading to a wide range of practical applications [6]. Despite these successes, PMS materials have an important shortcoming – their synthesis process requires rather harsh conditions (high temperature and pressure, very high or very low pH, toxic chemicals), resulting in unsustainable methods that cannot be adopted economically at industrial scales. This opened up a new area of research aiming to produce controlled nanoporous silica materials using environmentally friendly synthesis conditions [7, 8]. Shortly after the discovery of PMS, Tanev and Pinnavaia [9] made the first attempt towards this goal by synthesising Hexagonal Mesoporous Silica (HMS) materials using alkylamines as templates instead of ammonium surfactants, based on a hypothesised "neutral templating mechanism". Interestingly, amine-rich peptides and long-chain polyamines have later been shown to play a crucial role in directing the porous structure formation in biosilicification by marine organisms like diatoms and sponges [10-12], a process that leads to the formation of hierarchical structures of amazing beauty and complexity at very mild conditions of pressure, temperature and pH. Currently, amine-based "additives" are at the core of the rapidly expanding field of bio-inspired silica synthesis, which aims to adapt the principles of biosilicification to produce synthetic silica materials of controlled porosity under mild conditions with a low environmental footprint [8, 13].

The main bottleneck hindering further progress in this field is the lack of in-depth understanding of the underlying mechanism of amine-templated silica synthesis [4, 8]. In this paper, we shed new light on this issue through a combination of experimental studies and multi-scale modelling, focussing on HMS [9] as the first example of synthetic amine-templated silica material. Tanev and Pinnavaia [14] originally hypothesised that the self-assembly of the templated mesostructure, which ultimately controls the material properties, was governed by non-ionic interactions between neutral amine surfactant head groups and neutral silicates in solution. According to those authors, hydrogen-bond interactions promoted the formation of rod-like micelles and their organisation into hexagonal mesophases, which led them to argue that this represented the first example of a "neutral templating route" to the synthesis of ordered mesoporous silica [9], in marked contrast with the "ionic" templating route of PMS materials [2]. The proposed neutral templating mechanism was considered revolutionary at the time, as it implied that ordered mesoporous silica could be synthesised at near-neutral pH. However, the pH of the synthesis solution was

never reported in the original papers or in subsequent studies of these systems, and the underlying assumptions of the mechanism remained untested. Despite this fact, the neutral templating route has been tacitly accepted by the material science community, as evidenced in several reviews of the topic [6, 7, 15].

Support for the proposed neutral mechanism was mostly indirect, based on the idea that weaker template-silica hydrogen-bond interactions, relative to the stronger ionic interactions present in PMS synthesis solutions, would lead to the observed thicker pore walls and lower degree of order [14]. Here, the nature of the interactions between silicates and amine templates during the self-assembly of these materials was investigated through a combination of titration measurements, NMR analysis and molecular dynamics (MD) simulations. Our results indicate that the majority of amine templates are positively charged at the conditions of synthesis, and provide evidence for a charge-matching mechanism at the origin of the self-assembly of HMS materials. This new insight has potentially profound implications for our understanding of amine-templated silica synthesis, including naturally occurring and bio-inspired hierarchical silica materials.

HMS was originally prepared by dissolving TEOS (tetraethylorthosilicate) and primary amine surfactants with variable alkyl chain lengths ($NH_2C_nH_{2n+1}$, where n was between 10 and 18 carbon atoms) in a mixture of water and ethanol at temperatures ranging from ambient to 80 °C, with a typical composition being reported as 1.0 TEOS : 0.27 DDA : 9.09 EtOH : 29.6 H_2O, where DDA is dodecylamine (n=12 in the above amine chemical formula) [14]. We first performed acid-base titrations of DDA in a 50% v/v water/ethanol solution (equivalent to the above molar ratios) using 1M HCl, shown in Figure 1a (see Supporting Information for details). The titration found the pKa to be 10.00, corresponding to 9.8 after correction for the non-aqueous composition [16]. This result is somewhat lower than the literature value of 10.63 [17], measured in aqueous solution, but this is likely due to the relatively high alcohol concentration; the same effect has been observed previously for alkylamine molecules in the presence of methanol [18].

We then proceeded to measure the pH of different solutions considered in the Tanev and Pinnavaia study: 1) initial reaction solvent with DDA but before the addition of any TEOS; 2) reaction mixture immediately after the addition of TEOS to the solution in 1); 3) deliberately acidified DDA solution obtained by adding HCl to the solution in 1). The solution conditions are precisely the same as reported in the original study, and we have confirmed that the

synthesis solution led to the formation of HMS material with porosity, morphology and adsorption characteristics that are very similar to the original materials reported by Tanev and Pinnavaia (see Figure S1 and associated discussion). The results of these measurements are overlaid on the titration curve of Figure 1a, showing that the addition of acidic TEOS significantly lowers the pH of the initial solution to 9.2, after correcting for the non-aqueous composition. This is in very good agreement with a theoretical estimate of 8.9, obtained using literature values for the pKa of DDA (10.63 [17]) and of silicic acid (9.5 for the first deprotonation and 12.6 for the second deprotonation [19]). More importantly, it is sufficiently below the measured amine pK_a to indicate that a large majority of DDA molecules (at least 80%) will be positively charged at the start of the synthesis. Furthermore, we estimate, using the Henderson-Hasselbalch equation, that the charged amines will initially be in contact with approximately 77% neutral and 23% anionic silica monomers [20]. This is a far cry from the hypothesised "neutral" conditions in the original paper.

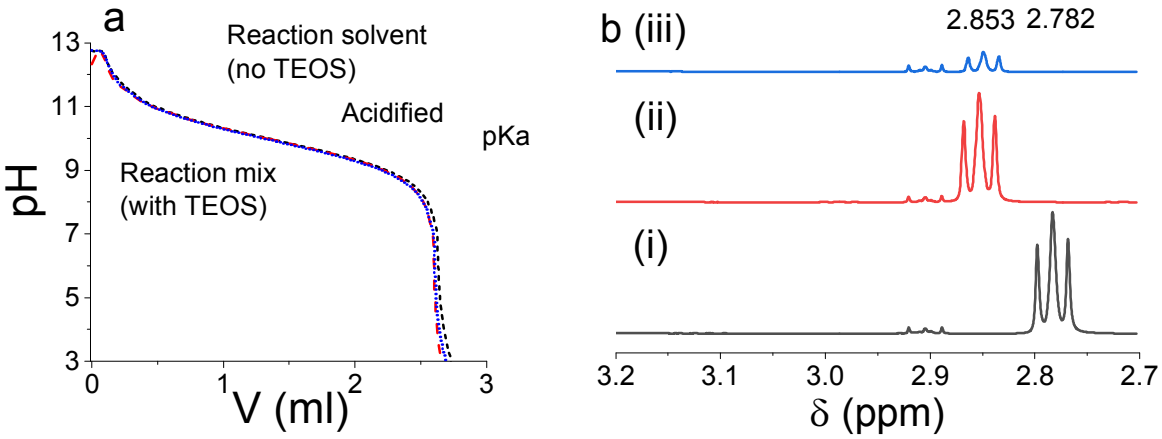

Figure 1 *– (a) Titrimetric determination, in triplicate, of DDA pKa in 50%v EtOH/H_2O mixture (initially 0.27 DDA: 9.09 EtOH: 29.6 H_2O by moles), overlaid with measured pH values from the reaction solvent (0.27 DDA: 9.09 EtOH: 29.6 H_2O by moles), acidified reaction solvent as described by Tanev and Pinnavaia [14] (0.27 DDA: 0.054 HCl: 9.09 EtOH: 29.6 H_2O by moles), and reaction mixture (1.0 TEOS: 0.27 DDA: 9.09 EtOH: 29.6 H_2O by moles). (b) (i) Comparison of ^1H NMR spectra for the reaction solvent, (ii) acidified reaction solvent, and (iii) reaction mixture solutions shown in figure (a). Overlay lines indicate the peak shift due to partial acidification of DDA relative to an external standard, which is similar for both the acidified reaction solvent and reaction mixture.*

Tanev and Pinnavaia carried out ^{14}N nuclear magnetic resonance (NMR) measurements on the synthesis solutions and on a deliberately acidified solution without silica. The fact that the acidified solution showed a strong NMR signal while no such signal was observed in any of the synthesis solutions led those authors to conclude that DDA was predominantly uncharged

during the synthesis of HMS, thus supporting the postulated neutral templating mechanism [14]. However, our titration results clearly show that the pH of the synthesis solution is lower than that of the "acidified" HCl-DDA mixture (see Figure 1a), a factor seemingly unaccounted for in the original paper. To support our titration measurements, we performed ^{1}H NMR measurements of DDA solutions under a range of conditions. Unlike the ^{14}N findings of Tanev and Pinnavaia, we were able to detect peaks corresponding to the C1 protons (linked to carbon atoms closest to the amine nitrogen; see SI for details) in all cases. These peaks were all shifted differently from an unmodified solution of DDA, indicating a different electronic environment in all cases (Figure 1b). Notably, this included a significant shift upon addition of TEOS to the DDA in EtOH/H_2O (and hence during HMS synthesis), similar to the shift observed upon partial acidification, and contrary to the conclusions of Tanev and Pinnavaia. Other modifications to the solution corresponding to changes in the ionic strength, DDA concentration or change in solvent composition during synthesis were then prepared and analysed to determine their effect on C1 peak shifting. Acidification was the only parameter that produced peak shifting of the magnitude seen in the reaction mixture (Figure S2).

Taken together, our results of acid-base titrimetry and ^{1}H NMR provide a clearer understanding of DDA chemistry during HMS synthesis than was previously possible. Whereas previous ^{14}N NMR experiments could only indicate the presence of protonated DDA, using ^{1}H NMR enables estimation of the degree of protonation based on the amine moiety's inductive effect. Using identical synthesis conditions to those previous studies, results from the ^{1}H NMR show that DDA molecules are predominantly in the protonated state during HMS synthesis, in marked contrast to the assertions of Tanev and Pinnavaia [9, 14]. The observed presence of large amounts of protonated DDA in both solutions strongly indicates that the origin of the different signals in their ^{14}N NMR measurements cannot be ascribed to different protonation states of the amine surfactants, as originally argued. A possible explanation is related to the pH-dependency of proton exchange rate and its peak-broadening effect. Rapid exchange of protons between protonated dodecylamine and water will lead to peak suppression, as the longevity of protonated dodecylamine species would be shorter than the ^{14}N chemical shift time scale. The pH-sensitivity of this phenomenon has been recently observed for the amine moiety in arginine over a narrow pH range [21], suggesting that the appearance of the ^{14}N peak in the previous work may have been due to the deceleration of exchange rate as the pH was lowered under acidified conditions, rather than

due to changes in the amine protonation state. It is also possible that the tetrahedral symmetry of the protonated amine group is distorted in the synthesis solution due to close interactions with silicates (see below), thus interfering with the ^{14}N NMR signal.

Our experimental measurements suggest that the system will be dominated by strong charge-charge interactions between silica and surfactants, and therefore the mechanism cannot occur on a neutral basis as originally assumed. To clarify the nature of the molecular-level interactions taking place in the synthesis solution, we carried out simulations using a multi-scale modelling approach. In brief, quantum-mechanical calculations [22] were used to obtain parameters for classical atomistic models of silicates in solution [23], which were then combined with atomistic models of water [24] and amine surfactants [25]. Parameters of a coarse-grained model of the system, based on the MARTINI approach [26], were then calibrated so that micelle density profiles and other structural properties matched those of the atomistic simulations. This approach has been successfully validated and applied to elucidate the self-assembly mechanism in the synthesis of PMS materials [23, 27-30] as well as of their organosilica derivatives [4, 31]. Details of the model parameterisation and validation procedure for HMS precursor solutions, including a diagram of the mapping scheme (Figure S5) and a table with the final set of parameters (Table S7), are provided in Supporting Information.

We began by carrying out simulations of a reference solution containing only water and DDA surfactants with a concentration of 0.22 M, which corresponds to the concentration used by Tanev and Pinnavaia, at different pH values. At a pH below 8, essentially all surfactants are charged (see Figure 1a), and they self-assemble into small micelles of nearly spherical shape (Figure 2a). The average aggregation number of these micelles (80) is quite close to that observed experimentally (68) [32], thus validating our coarse-grained model for the surfactant solutions. Conversely, when the pH is above 12, virtually all surfactants are neutral (Figure 1a). In this case, the system phase-separates into a pure solvent and a pure-surfactant phase, the latter being composed of a single completely disordered aggregate (Figure 2b). This also mirrors experimental observations, which show that DDA in the neutral form is insoluble in pure water at ambient conditions [33].

When TEOS is added to the DDA/water solution at the start of the HMS synthesis, the pH drops to 9.2, as described above. As such, the majority of DDA molecules will be protonated (Figure 1a) and the starting surfactant configuration will be similar to that shown in Figure

2a. The pH is also high enough that we can consider the hydrolysis of TEOS, yielding monosilicic acid and ethanol, to be rapid and complete [34]. Simulations of a solution of DDA and silica monomers with the speciation corresponding to the experimental pH (see SI for details) gives rise to the formation of rod-like micelles (Figure 2c). The sphere-to-rod transition upon addition of TEOS is caused by the strong electrostatic attraction between anionic silica and cationic surfactant heads. Indeed, a detailed analysis of the simulations leading to the structure shown in Figure 2c reveals that surfactant head groups interact predominantly with anionic silicates, while neutral silicates are practically absent from their immediate vicinity (Figure S16). As anionic silicates adsorb at the micelle surface, they screen the repulsion between positively charged head groups, reducing the equilibrium curvature of the aggregates [35]. A similar mechanism was observed in the early stages of the synthesis of PMS materials from permanently ionised ammonium surfactants [28]. Thus, the presence of anionic silica is shown to induce profound changes to the equilibrium surfactant structures, supporting a co-operative templating mechanism akin to that of PMS [3, 29].

Interestingly, when neutral silica monomers were added to a solution containing only neutral surfactants, in an attempt to mimic the hypothesised neutral templating route, very little adsorption of silica at the surface of the surfactant aggregate was observed. Instead, silicates mostly remain in the aqueous phase and appear to have no effect on the phase separation of the insoluble surfactants (Figure 2d). Simulations of a smaller version of this system at the atomistic level of detail showed that neutral silicates do indeed form hydrogen bonds with neutral amine surfactants, but these are much weaker than bonds formed between either of those molecules with water (Figure S17). This explains why neutral silica monomers prefer to stay in the bulk solution, and further supports our argument that hydrogen-bond interactions between neutral species could not constitute a driving force for inducing mesophase formation in HMS synthesis.

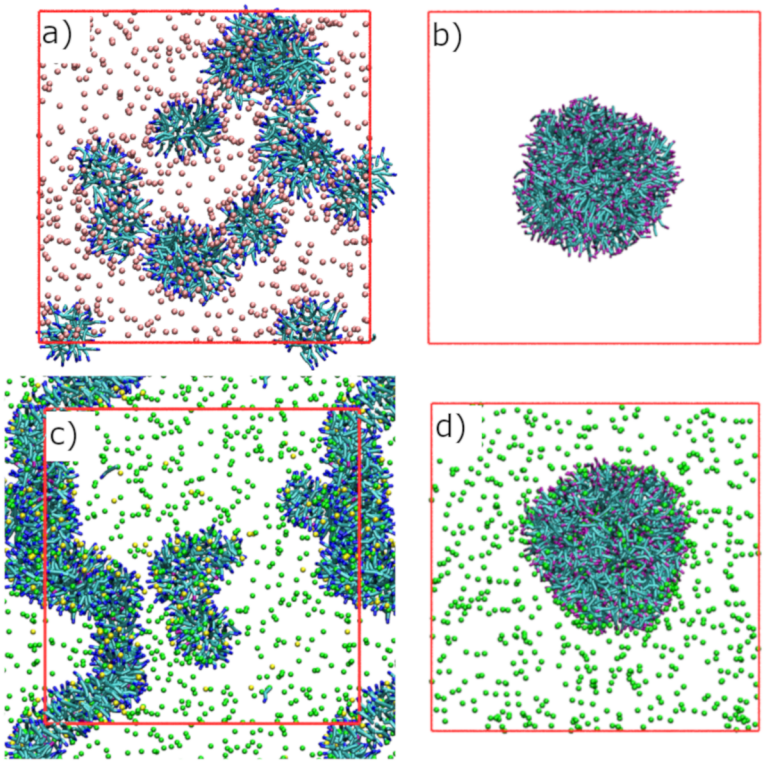

Figure 2 – *Simulation snapshots obtained for aqueous DDA solutions at 0.22 M: (a) charged surfactants without silica (pH < 8); (b) neutral surfactants without silica (pH > 12); (c) charged (89%) and neutral (11%) surfactants with 23% anionic silica monomers and 77% neutral silica monomers (pH ~9.2); (d) neutral surfactants with 100% neutral silica monomers (hypothetical conditions). Water has been removed for clarity. Some of the snapshots include part of their periodic images to aid visualisation. Colour code is: DDA+ heads, blue; DDA heads, purple; DDA+ and DDA tails, teal; chloride, pink; anionic silica monomers (SiO^-), yellow; neutral silica monomers (SiO^0), green. The red box represents the boundary of the simulation cell, which in all cases is close to 20 nm side (Table S8).*

It has previously been shown that the presence of silica oligomers (at least 30% of dimers) was necessary to promote the formation of a hexagonal mesophase in the synthesis of PMS from cationic ammonium surfactants [29]. In the case of HMS, a similar conclusion can be drawn from our simulations. When silicates remain in the monomeric form, long rod-like micelles are formed (Figure 2c), but no evidence for the formation of an ordered array of micelles is seen. In contrast, when the monomers are replaced by dimers, meant to represent a later stage of the synthesis after silica has been allowed to polymerise to some extent, the micelles begin to aggregate. This tendency for micelles to aggregate can already be seen at low silica/surfactant ratios (Figure 3a), and becomes increasingly dominant as the concentration of silica increases (Figures 3b).

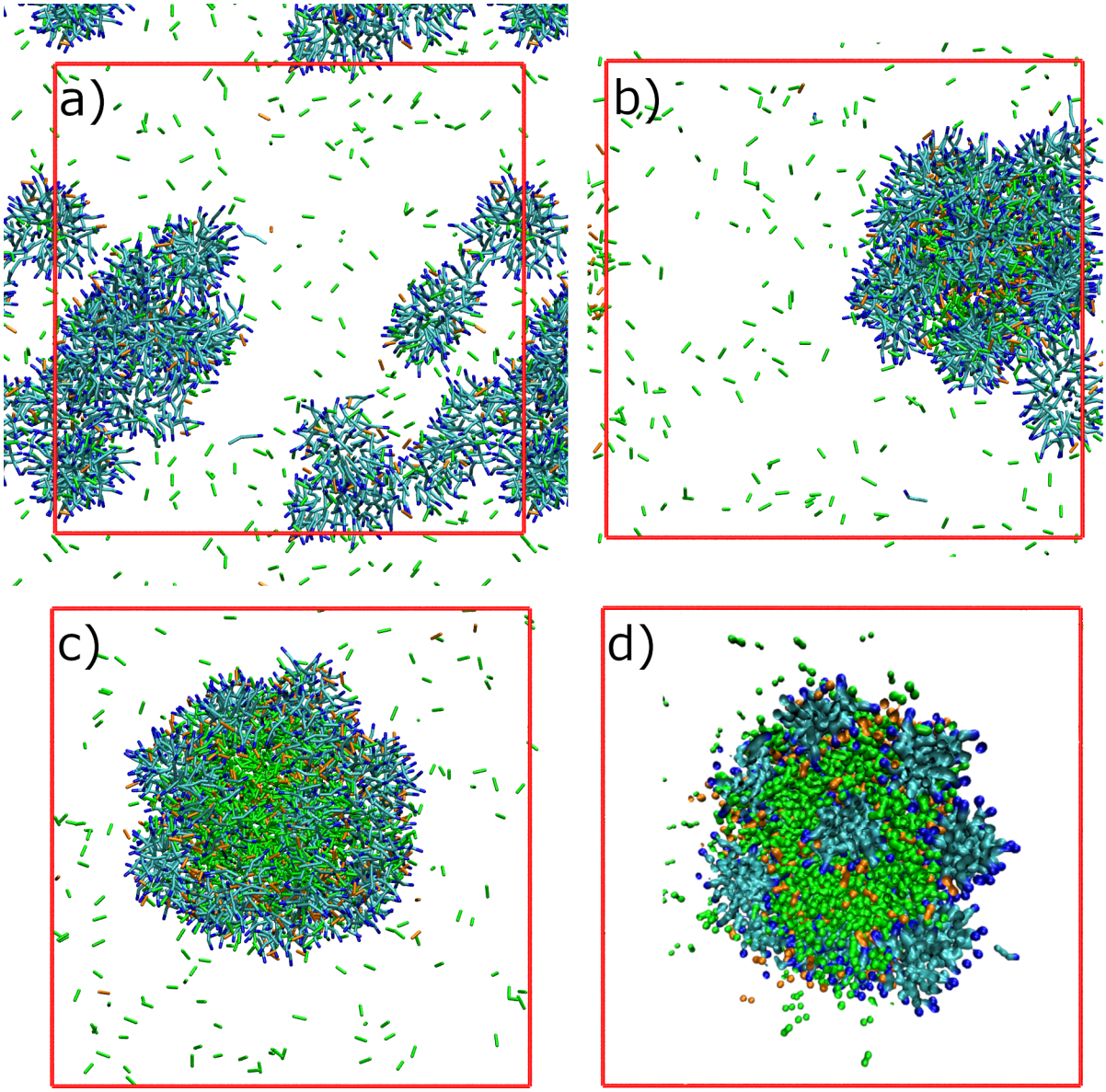

Figure 3 *– Simulation snapshots obtained for surfactant/silica solutions with neutral and singly-charged silica dimers, at increasing silica:surfactant ratios: a) 1:1; b) 2:1; c) 4:1; d) cross-section of the aggregate obtained at a 4:1 ratio. Water and chloride ions have been removed for clarity. Some of the snapshots include part of their periodic images to aid visualisation. Colour code is: DDA+ heads, blue; DDA+ tails, teal; chloride, pink; anionic dimers, orange; neutral dimers, green. The red box represents the boundary of the simulation cell, which in all cases is close to 20 nm side (Table S8).*

In the original study of Tanev and Pinnavaia, using a silica/surfactant ratio of approximately 4:1 [14], the authors argued, through X-ray diffraction (XRD) and transmission electron microscopy (TEM) characterisation, that their materials possessed a long-range hexagonally ordered array of cylindrical pores, similar to that of PMS materials synthesised from alkylammonium surfactants, but with thicker and hence more stable pore walls. However,

subsequent work by the same group [36] and by others [37, 38] showed that in fact the pore structure of HMS was more akin to a rather disordered packing of wormlike micelles, instead of the regular hexagonal packing of cylinders observed in PMS materials. Our simulations under similar conditions (Figure 3c) show the formation of a roughly hexagonal array of elongated micelles – Figure 3d shows the nearly spherical cross-section of each micelle (in blue) surrounded by a thick layer of silica (in orange and green). Interestingly, the degree of order of the HMS precursor mesophase is much lower than observed in the case of PMS [29], but the silica walls are significantly thicker. Both these observations are in strong qualitative agreement with available experimental information about the pore network structure of HMS materials [36, 37].

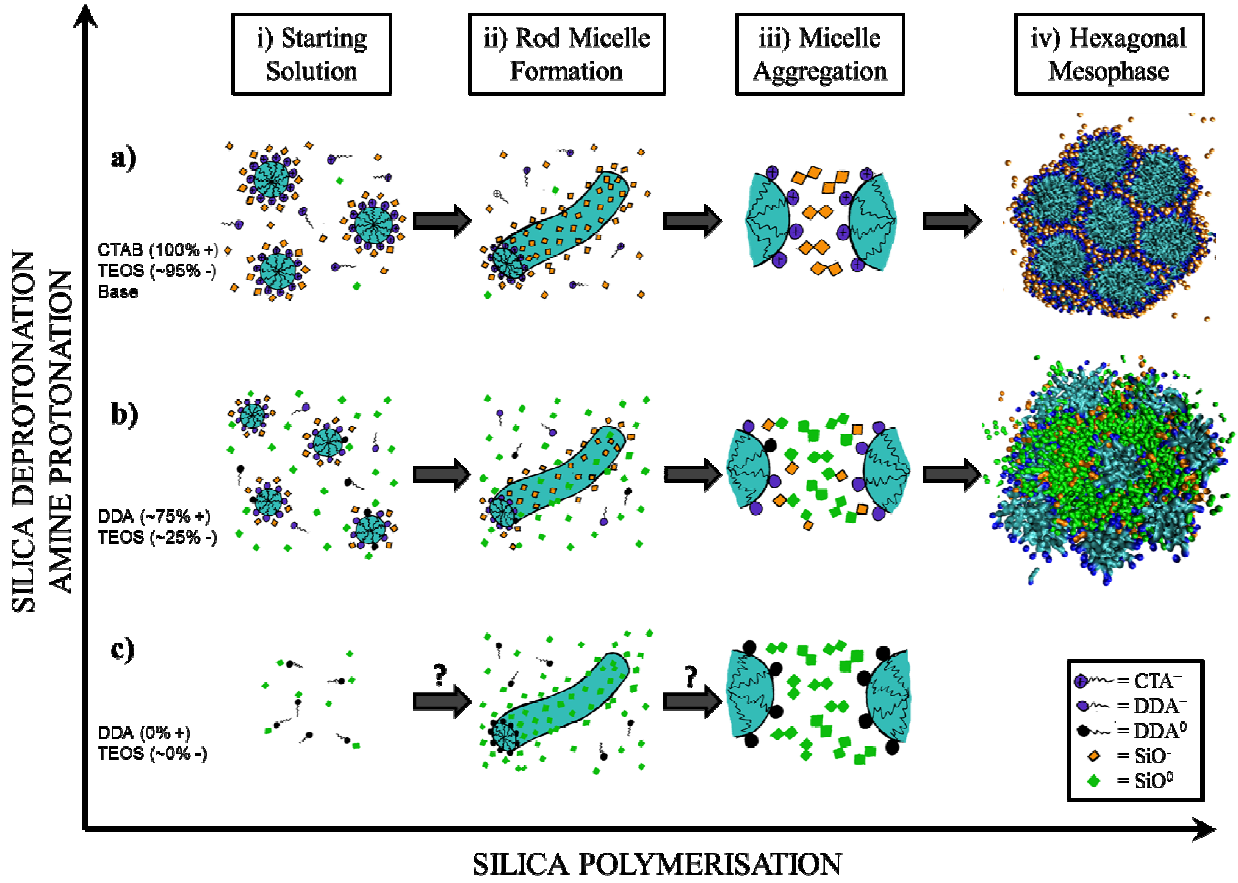

Figure 4 *– Diagram depicting different mechanisms for the synthesis of mesostructured silica materials: a) PMS synthesis at high pH [29]; b) HMS synthesis (this paper); c) hypothetical neutral templating route to HMS [14]. The composition and approximate speciation of the initial solution is given at the start for each mechanism. Colour code is: surfactant heads, blue; surfactant tails, teal; anionic silicates, orange; neutral silicates, green. In the schematic drawings (see legend), cationic ammonium surfactants are represented by crossed circles, cationic amine surfactants by open circles, and neutral amines by black circles. The hexagonal mesophases are represented by snapshots obtained from our simulations.*

In Figure 4, we also contrast our proposed mechanism for HMS synthesis, based on charge-matching (path b) with the hypothetical neutral templating mechanism (path c) proposed by Tanev and Pinnavaia [9, 14]. Those authors suggest that neutral silicates interact with neutral amines through hydrogen bonds in the initial synthesis solution (step i), leading to the formation of rod-like micelles. However, Tanev and Pinnavaia do not offer a conclusive explanation for how the weak hydrogen-bond interactions would lead to the formation of rod-like micelles (step ii) for a surfactant that, under normal circumstances, would form small spherical aggregates. As we have demonstrated above, such weak interactions are relatively rare in the synthesis solution and are highly unlikely to induce any changes in the amine aggregation state. Conversely, rod-like structures arise naturally in our mechanism due to the effective reduction in charged amine head group size brought about by the adsorption of anionic silicates at the micelle surface. Similarly, Tanev and Pinnavaia do not explain in detail how the rod-like micelles are subsequently led to aggregate, stating merely that it arises due to "further silica condensation" [14]. Based on experimental and simulation results, we propose that such aggregation, leading to the formation of a loosely hexagonally-ordered mesophase, arises from a combination of strong charge-matching interactions and reduced silica solubility as the degree of condensation increases.

To summarize, our combined experimental and multi-scale modelling study has elucidated the synthesis mechanism of the earliest examples of mesoscale ordered silica materials in unprecedented molecular detail. Crucially, our results contradict the originally postulated, and widely accepted, neutral templating mechanism for HMS synthesis. Instead, acid-base titration and NMR measurements show that amine surfactants are mostly cationic when silica is added to the synthesis mixture, while the modelling shows that it is the charge-matching interactions between surfactants and anionic silicates that control the first stages of formation of HMS precursor mesophases. These interactions effectively screen the repulsion between initially spherical micelles, promoting a sphere-to-rod transition shortly after the addition of silica, when the latter is still in monomeric form. As silica polymerizes, hydrophobic interactions between neutral and anionic silicates begin to play a role, promoting the aggregation of worm-like micelles into a phase-separated mesophase with loosely hexagonal order. The higher concentration of silica necessary to aggregate the micelles leads to materials with relatively thick pore walls and relatively low degree of order, when compared to their PMS counterparts, in agreement with experimental characterisation.

Although our study focused on a particular example of porous silica, our conclusions regarding the importance of charged interactions are likely to be general for this class of materials, and beyond, given the widespread use of amine templating to produce a range or porous materials (TiO_2, ZrO_2, etc.) [40]. Indeed, our previous atomistic simulations of MSU-V [41], which is a similar material to HMS but synthesised from double-headed amine surfactants that form multi-layered vesicular structures [42], showed that its synthesis mechanism is also controlled by charge-matching interactions instead of the originally hypothesised weak hydrogen bonds. Furthermore, our results are relevant to the study of bioinspired silicas, which use amine molecules to control the reaction and product properties [13]. Our recent study of template removal in bioinspired silica synthesised from polyamine templates also demonstrated the key role played by ionic silica-amine interactions in the synthesis process [43]. Taken together, this evidence indicates we should rethink the prevailing views about how these increasingly important materials are synthesised. Crucially, in all of the above examples, the synthesis is found to be heavily dependent on the pH of the precursor solution. This opens up interesting new routes to controlling the pore structure of industrial-grade silica. For example, it may be possible to synthesise a family of porous silicates and non-silicates with increasing degree of order by tuning the template self-assembly by slightly increasing the pH - i.e. operating somewhere between the two mechanisms depicted in Figure 4a-b. Also, adding a small percentage of permanently ionised surfactants, like quaternary alkylammonium, may increase the degree of order of the material. Further, by combining the findings reported herein with the recent developments on room temperature synthesis of porous silica [8] and eco-friendly removal of templates [43] has the potential to deliver commercially viable manufacturing routes to porous materials. Research along these lines is currently being explored in our laboratories.

Supporting Information:

Experimental details and additional results; technical details and force field parameters for atomistic simulations; technical details and force field parameters for coarse-grained simulations; parameterization procedure of the coarse-grained model; additional simulation results. All the input files for the simulations presented herein are freely available to download from the University of Strathclyde data repository: DOI: 10.15129/8f589df4-a60e-4af1-bd24-d3376c25eea9.

Acknowledgements:

MJ acknowledges financial support from EPSRC UK (Project Grant EP/L014297/1). AC is grateful to the University of Strathclyde for a Ph.D. studentship. SP thanks financial support by the host department and EPSRC (EP/L017059/1 and EP/P006892/1). Results were obtained using the ARCHIE-WeSt High Performance Computer (www.archie-west.ac.uk) funded by EPSRC grant no. EP/K000586/1. The authors are also grateful to Germán Pérez-Sánchez for providing a snapshot of the PMS material, included in Figure 4.

Competing Interests: The authors declare no competing interests.

References

1 - Beck, J. S. et al. A new family of mesoporous molecular sieves prepared with liquid crystal templates. *J. Am. Chem. Soc.* **114**, 10834-10843 (1992).

2 - Monnier, A. et al. Cooperative formation of inorganic-organic interfaces in the synthesis of silicate mesostructures. *Science* **261**, 1299-1303 (1993).

3 - Firouzi, A.; Atef, F.; Oertli, A. G.; Stucky, G. D.; Chmelka, B. F. Alkaline Lyotropic Silicate−Surfactant Liquid Crystals. *J. Am. Chem. Soc.* **119**, 3596–3610 (1997).

4 - Jorge, M. et al. Modelling the self-assembly of silica-based mesoporous materials. *Mol. Simul.* **44**, 435-452 (2018).

5 - Barton, T. J. et al. Tailored Porous Materials. *Chem. Mater.* **11**, 2633–2656 (1999).

6 - Wan, Y.; Zhao, D. On the Controllable Soft-Templating Approach to Mesoporous Silicates. *Chem. Rev.* **107**, 2821-2860 (2007).

7 - Gérardin, C.; Reboul, J.; Bonne, M.; Lebeau, B. Ecodesign of ordered mesoporous silica materials. *Chem. Soc. Rev.* **42**, 4217-4255 (2013).

8 - Patwardhan, S.V.; Manning J. R. H.; Chiacchia, M. Bioinspired synthesis as a potential green method for the preparation of nanomaterials: Opportunities and challenges. *Curr. Op. Green Sus. Chem.* **12**, 110-116 (2018).

9 - Tanev, P. T.; Pinnavaia, T. J. A Neutral Templating Route to Mesoporous Molecular Sieve. *Science* **267**, 865-867 (1995).

10 - Sumper, M.; Kröger, N. Silica formation in diatoms: the function of long-chain polyamines and silaffins. *J. Mater. Chem.* **14**, 2059-2065 (2004).

11 - Gröger, C.; Lutz, K.; Brunner, E. Biomolecular self-assembly and its relevance in silica biomineralization. *Cell Biochem. Biophys.* **50**, 23-39 (2008).

12 - Hildebrand, M.; Lerch, S. J. L.; Shrestha, R. P. Understanding Diatom Cell Wall Silicification—Moving Forward. *Front. Mar. Sci.* **5**, 125 (2018).

13 - Patwardhan, S. V. Biomimetic and bioinspired silica: recent developments and applications. *Chem. Commun.* **47**, 7567-7582 (2011).

14 - Tanev, P. T.; Pinnavaia, T. J. Mesoporous Silica Molecular Sieves Prepared by Ionic and Neutral Surfactant Templating: A Comparison of Physical Properties. *Chem. Mater.* **8**, 2068–2079 (1996).

15 - Soler-Illia, G. J. A. A.; Sanchez, C.; Lebeau, B.; Patarin, J. Chemical Strategies To Design Textured Materials: from Microporous and Mesoporous Oxides to Nanonetworks and Hierarchical Structures. *Chem. Rev.* **102**, 4093-4138 (2002).

16 - Gelesma, W. J.; de Ligny, C. L.; Remijnse, A. G.; Blijleven, H. A. pH-Measurements in alcohol-water mixtures, using aqueous standard buffer solutions for calibration. *Recl. Trav. Chim. Pays-Bas* **85**, 647-660 (1966)

17 - Perrin, D. D. *Dissociation constants of organic bases in aqueous solution: supplement.* (Butterworths, London, 1972).

18 - Ohtaki, H.; Maeda, M. Ionic Equilibria in Mixed Solvents. VIII. Solvent Effects on the Dissociation of Diprotic Acids in Aqueous Methanol Mixtures. *Bull. Chem. Soc. Japan* **46**, 2052–2056 (1973).

19 – Sefcík and McCormick [20], upon reviewing equilibrium constants for reactions involving small silicates (monomers, dimers, etc.), reported a pKa of 9.5 for monosilicic acid, which is refined from the value of 9.8 reported by Iler in his earlier monograph [34].

20 - Sefcík, J.; McCormick, A. V. Thermochemistry of aqueous silicate solution precursors to ceramics. *AIChE J.* **43**, 2773-2784 (1997).

21 - Khirich, G.; Holliday, M. J.; Lin, J. C.; Nandy, A. Measurement and Characterization of Hydrogen–Deuterium Exchange Chemistry Using Relaxation Dispersion NMR Spectroscopy. *J. Phys. Chem. B* **122**, 2368–2378 (2018).

22 - Gomes, J. R. B.; Cordeiro, M. N. D. S.; Jorge, M. Gas-phase molecular structure and energetics of anionic silicates. *Geochim. Cosmochim. Acta* **72**, 4421-4439 (2008).

23 - Jorge, M.; Gomes, J. R. B.; Cordeiro, M. N. D. S.; Seaton, N. A. Molecular Dynamics Simulation of the Early Stages of the Synthesis of Periodic Mesoporous Silica. *J. Phys. Chem. B* **113**, 708-718 (2009).

24 - Berendsen, H. J. C.; Grigera, J. R.; Straatsma, T. P. The missing term in effective pair potentials. *J. Phys. Chem.* **91**, 6269-6271 (1987).

25 - Jorgensen, W. L.; Maxwell, D. S.; Tirado-Rives, J. Development and Testing of the OPLS All-Atom Force Field on Conformational Energetics and Properties of Organic Liquids. *J. Am. Chem. Soc.* **118**, 11225-11236 (1996).

26 - Marrink, S. J.; Risselada, H. J.; Yefimov, S.; Tieleman, D. P.; de Vries, A. H. The MARTINI Force Field: Coarse Grained Model for Biomolecular Simulations. *J. Phys. Chem. B* **111**, 7812-7824 (2007).

27 - Jorge, M.; Gomes, J. R. B.; Cordeiro, M. N. D. S.; Seaton, N. A. Molecular Simulation of Silica/Surfactant Self-assembly in the Synthesis of Periodic Mesoporous Silicas. *J. Am. Chem. Soc.* **129**, 15414-15415 (2007).

28 - Pérez-Sánchez, G.; Gomes, J. R. B.; Jorge, M. Modeling Self-Assembly of Silica/Surfactant Mesostructures in the Templated Synthesis of Nanoporous Solids. *Langmuir* **29**, 2387-2396 (2013).

29 - Pérez-Sánchez, G. et al. Multiscale Model for the Templated Synthesis of Mesoporous Silica: The Essential Role of Silica Oligomers. *Chem. Mater.* **28**, 2715-2727 (2016).

30 - Chien, S.-C. et al. Molecular Simulations of the Synthesis of Periodic Mesoporous Silica Phases at High Surfactant Concentrations. *J. Phys. Chem. C **121***, 4564–4575 (2017).

31 - Futamura, R.; Jorge, M.; Gomes, J. R. B. Role of the organic linker in the early stages of the templated synthesis of PMOs. *Phys. Chem. Chem. Phys.* **15**, 6166-6169 (2013).

32 - Malliaris, A.; Le Moigne, J.; Sturm, J.; Zana, R. Temperature dependence of the micelle aggregation number and rate of intramicellar excimer formation in aqueous surfactant solutions. *J. Phys. Chem.* **89**, 2709–2713 (1985).

33 - Broome, F. K.; Hoerr, C. W.; Harwood, H. J. The Binary Systems of Water with Dodecylammonium Chloride and Its N-Methyl Derivative. *J. Am. Chem. Soc.* **73**, 3350-3352 (1951).

34 - Iler, R. K. *The Chemistry of Silica: Solubility, Polymerization, Colloid and Surface Properties, and Biochemistry.* (Wiley-Interscience, New York, 1979).

35 - Israelachvili, J. N. *Intermolecular and Surface Forces*. (Academic Press, New York, 1985).

36 - Zhang, W.; Pauly, T. R.; Pinnavaia, T. J. Tailoring the Framework and Textural Mesopores of HMS Molecular Sieves through an Electrically Neutral (S°I°) Assembly Pathway. *Chem. Mater.* **9**, 2491-2498 (1997).

37 - Caldararu, H.; Caragheorgheopol, A.; Savonea, F.; Macquarrie, D. J.; Gilbert, B. C. A Spin Probe Study of Mesoporous Silica Formation via a Neutral Templating Route. *J. Phys. Chem. B* **107**, 6032-6038 (2003).

38 - Galarneau, A. et al. Sponge Mesoporous Silica Formation Using Disordered Phospholipid Bilayers as Template. *The Journal of Physical Chemistry B* **114**, 2140–2152 (2010).

39 - Patwardhan, S. V.; Maheshwari, R.; Mukherjee, N.; Kiick, K. L.; Clarson, S. J. Conformation and Assembly of Polypeptide Scaffolds in Templating the Synthesis of Silica:

An Example of a Polylysine Macromolecular “Switch”. *Biomacromolecules* **7**, 491–497 (2006).

40 - Davis, M. E. Ordered porous materials for emerging applications. *Nature* **417**, 813-821 (2002).

41 - Centi, A.; Jorge, M. Molecular Simulation Study of the Early Stages of Formation of Bioinspired Mesoporous Silica Materials. *Langmuir* **32**, 7228-7240 (2016).

42 - Tanev, P. T.; Pinnavaia, T. J. Biomimetic Templating of Porous Lamellar Silicas by Vesicular Surfactant Assemblies. *Science* **271**, 1267-1269 (1996).

43 - Manning, J. R. H.; Yip, T. W. S.; Centi, A.; Jorge, M.; Patwardhan, S. V. An eco-friendly, tunable and scalable method for producing porous functional nanomaterials designed using molecular interactions. *ChemSusChem* **10**, 1683-1691 (2017).

Supporting Information: The Role of Charge-Matching in Nanoporous Materials Formation

Alessia Centi,[†] Joseph R. H. Manning,[‡] Vibha Srivastava,[‡] Sandra van Meurs,[¶] Siddharth V. Patwardhan,[*,‡] and Miguel Jorge[*,†]

[†]*Department of Chemical and Process Engineering, University of Strathclyde, 75 Montrose Street, Glasgow G1 1XJ*

[‡]*Department of Chemical and Biological Engineering, University of Sheffield, Mappin Street, Sheffield S1 3JD*

[¶]*Department of Chemistry, University of Sheffield, Brook Hill, Sheffield S3 7HF, United Kingdom*

E-mail: s.patwardhan@sheffield.ac.uk; miguel.jorge@strath.ac.uk

1 Experimental details

DDA titration pH titration tests on DDA were conducted using a Metrohm 902 Titrando system and Tiamo 2.5 software using the mono endpoint titration (MET) command. Using this, HCl at a concentration of 1 M was added at a constant rate (typically 50 µl/min) during which time the pH was recorded. To determine titration endpoints and hence species pK_a, $\frac{d^2pH}{dt^2}$ was numerically calculated in OriginPro 2017 using a Savitsky-Gorlay smoothing algorithm (the time derivative was used instead of the volume derivative to increase precision; as $\frac{dV}{dt}$ is constant, this does not affect determination of the inflection points). Inflection points

indicating the titration endpoint were then found by identifying the characteristic point on the second differential curve. From here, the pKa could be calculated as the pH after dosing half of the required acid, as exemplified in Figure 1-a in the main body.

HMS synthesis method Hexagonal mesoporous silica was synthesised according to the procedure first described by Tanev and Pinnavaia[1]. Dodecylamine (933 mg, 5 mmol) was dissolved in a mixture of ethanol (10.6 ml, 182 mmol) and water (10.6 ml, 589 mmol) under vigorous stirring at ambient temperature in a 180 ml polypropylene tub. TEOS (4.43 ml, 20 mmol) was then added in a single aliquot, and the tube sealed and left to age under stirring for 18 hours. After this time, the resultant coagulum was decanted into 50 ml centrifuge tubes and spun at 5000 g for 15 minutes three times, washing with water between each spin. After the final spin, the white slurry was scraped into a watch glass for air drying.

Activation of the HMS was performed by calcination at 550 °C in a muffle furnace for 12 hours, after which nitrogen adsorption analysis was performed to confirm that mesoporosity was incorporated successfully. The results of the BET analysis are shown in figure S1

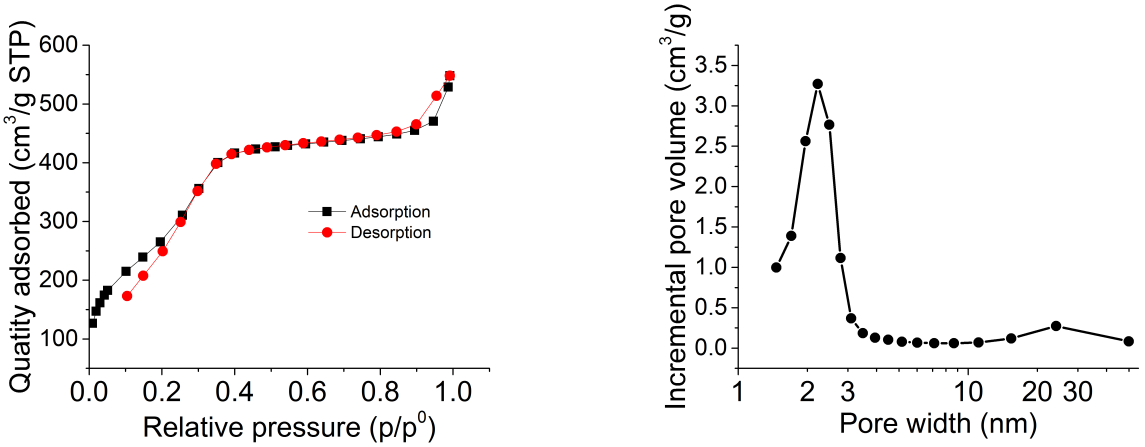

(a) (b)

Figure S1: Nitrogen adsorption data for HMS produced in this study: (a) experimental nitrogen isotherm at 77 K showing adsorption (black) and desorption (red), and (b) BJH pore-size distribution, showing a peak at 2.2 nm in accordance with reference[1]

.

Preparation of test DDA solutions for NMR analysis To test a range of solution environments for the DDA molecule and measure their relative NMR spectra compared to the reaction mixture, DDA solutions were made up spiked with HCl or NaCl. Further, a solution with low DDA concentration was made up to replicate the final concentration in the supernatant after HMS precipitation. Table S1 shows the compositions of the solutions used for direct NMR and pH analysis.

Table S1: Composition of various HMS reaction mixture mimics for NMR analysis

Component	Original reaction mixture[a]	DDA starting solution	Low concentration	NaCl doped	Post-hydrolysis solvent	20 % mol protonated[b]	90 % mol protonated[b]	99 % mol protonated[b]
DDA mg	933.1	49.6	25.0	164.8	24.8	49.5	164.7	163.5
(mmol)	(5.03)	(0.268)	(0.135)	(0.889)	(0.135)	(0.267)	(0.889)	(0.882)
NaCl mg	-	-	-	10.4	-	-	-	-
(mmol)	-	-	-	(0.179)	-	-	-	-
HCl ml[c]	-	-	-	-	-	0.054	0.800	0.890
(mmol)	-	-	-	-	-			
H_2O ml	10.6	0.533	1.75	1.75	1.635	0.479	0.955	0.865
(mmol)	(589)	(29.6)	(97.2)	(97.2)	(90.8)	(29.6)[d]	(97.5)[d]	(97.5)[d]
EtOH ml	10.6	0.531	1.75	1.75	2.515	0.531	1.75	1.75
(mmol)	(182)	(9.09)	(29.97)	(29.97)	(43.1)	(9.09)	(29.97)	(29.97)

[a] Containing 4.43 ml TEOS (20 mmol)
[b] as determined by the Henderson-Hasselbalch equation;
[c] volume of a 1M aqueous HCl solution
[d] including H_2O added with HCl

NMR investigation of HMS deshielding under different conditions Reaction supernatants and test solutions were loaded directly into standard 5 mm NMR tubes which were subsequently fitted with coaxial inserts containing 1 % w/w 4,4-dimethyl-4-silapentane-1-sulfonic acid (DSS) in D_2O to provide a deuterium lock and quantitation reference. NMR spectra were acquired using a Bruker AVANCE III HD spectrometer operating at 500.13 MHz, using a 30 degree flip angle for 16 transients, 10 kHz spectral window, 3.3 s acquisition time (64k points) plus 1 second relaxation delay.

Once collected, NMR shifts were normalised against the DSS trimethylsilyl peak. DDA concentration and chemical environment were analysed through the peak at $\delta \approx 2.78$ ppm, corresponding to the protons on the carbon closest to the amine functionality, referred to as C1 protons (the protons on the amine functionality were impossible to analyse due to their

high exchange frequency with water)[2].

Through the NMR experiments, neither concentration nor ionic strength were found to have a large effect on the DDA peak shifting, indicating that these variables could not be responsible for the observed shifting from $\delta = 2.78$ ppm to $\delta = 2.85$ ppm. The effect of TEOS hydrolysis on solvent environment was then investigated by changing the relative volumes of ethanol and water in the reaction mixture to correspond with complete hydrolysis and condensation of the TEOS (corresponding to molar concentrations of 0.04 DDA: 27.6 H_2O: 13.09 EtOH). This showed a larger effect, with the observed peak shifting to $\delta = 2.83$ ppm, although significantly this was still unable to replicate the peak shifting associated with the chemical reaction.

Despite this, acidification of the reaction mixture to 20 %, 90 %, and 99 % molar protonation was found to have a significant effect on DDA peak deshielding, with the peaks moving to 2.85, 3.12, and 3.14 ppm, respectively. This more than accounted for the shift in the C1 signal measured in the reaction supernatant, therefore it was concluded that a significant amount of protonation had occurred during the addition of TEOS. NMR spectra for the samples in different chemical environments is shown in Figure S2.

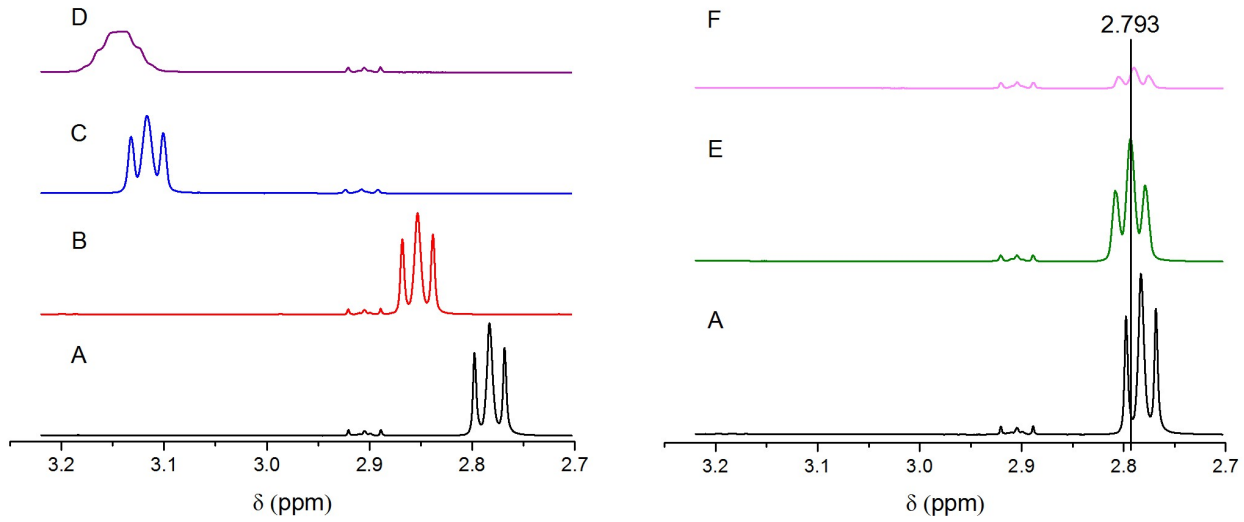

Figure S2: Comparison of NMR spectra taken for the different DDA solutions prepared in this study: (A) DDA starting solution, (B) NaCl doped, (C) Low concentration, (D) Post-hydrolysis solvent, (E) 20 % protonated, (F) 90 % protonated, (G) 99 % protonated. Vertical line represents major peak from reaction mixture at $\delta = 2.85$ ppm

2 Atomistic simulations

Water molecules were modelled using the SPC/E potential[3], while the OPLS all-atom force field[4,5] was used for surfactants and counter-ions. Figure S3 provides a representation of the two types of surfactant (neutal and cationic) considered. Label Hn represents hydrogen atoms belonging to amino groups, with N indicating a nitrogen and Cn a carbon bonded to it. The hydrogens on Cn atoms are referred as Hcn while those on carbons C and C3 in the hydrocarbon chain are called Hc. When the amine heads are charged, the hydrogen atoms in the amino groups take the name Hnc while the nitrogens are indicated by Nc and the carbons bonded to them by Cnc.

Parameters used for silica monomers and dimers were taken from the work of Jorge et al.[6]; a representation of all the inorganic species considered is provided in Figure S4. The nomenclature for silicates is as follows: SiN and SiI are used for neutral and anionic silicons

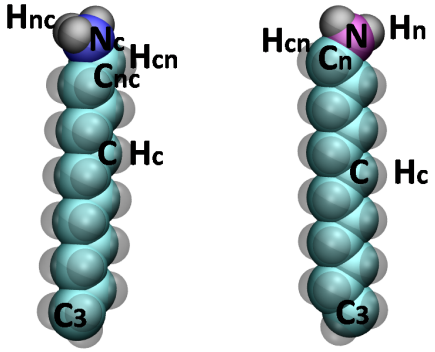

(a) DDA (b) DDA$^+$

Figure S3: All-atom representation of the dodecylamine surfactants in different charge states: neutral DDA surfactants (a) predominantly exist at high pH (> 12), while at pH lower than 8 only charged DDA$^+$ (b) are found. Neutral nitrogens, purple; charged nitrogens, blue; carbons, teal and hydrogens, gray.

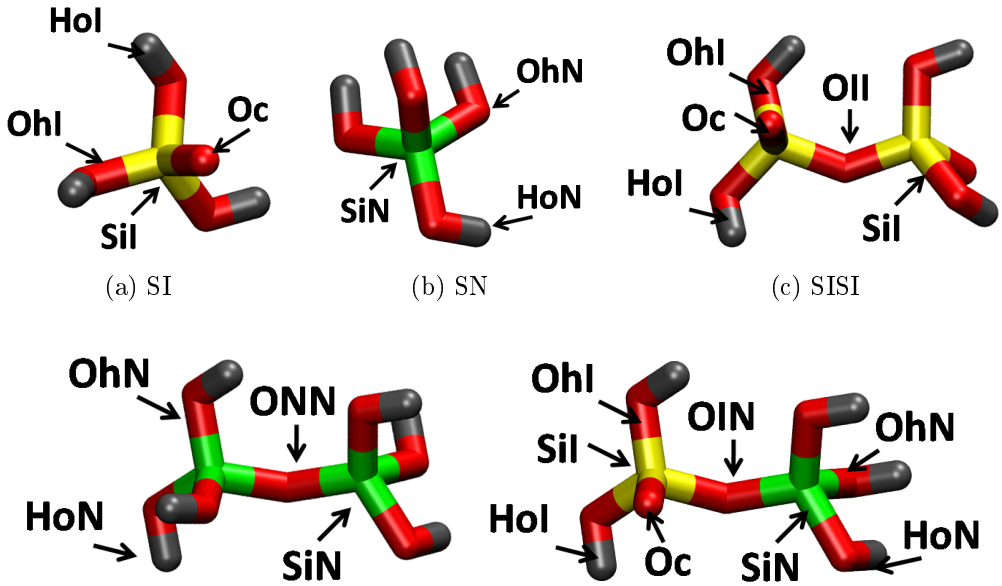

(a) SI (b) SN (c) SISI

(d) SNSN (e) SISN

Figure S4: All-atom representations of the different silicate species: SI, anionic monomer; SN, neutral monomer; SISI, dimer with two charges; SNSN, neutral dimer and SISN, dimer with one charge. Neutral silicons, green; charged silicons, yellow; oxygens, red and hydrogens, gray.

respectively, OhN and HoN for oxygen and hydrogen atoms belonging to hydroxyl groups in neutral species, while OhI and HoI are used for the corresponding atoms of hydroxyl groups when these are part of anionic species, Oc is a charged oxygen and finally OII, ONN, and OIN represent oxygen atoms linking, respectively, two anionic silicons, two neutral silicons, or one anionic and one neutral silicon.

Tables S2- S5 contain all force field parameters used for atomistic simulations. The potential energy function is represented as the sum of angle bending, dihedral torsion, Lennard-Jones interactions and Coulomb electrostatic terms. Non-bonded interactions are calculated only for atoms that are separated by three or more bonds, while the 1-4 interactions are scaled down by a factor of 0.5. Bond lengths were constrained by applying the LINCS algorithm[7], a cutoff of 1.2 nm was applied to short-range dispersion interactions and the same distance for the particle-mesh Ewald method (PME)[8,9] to take into account the long-range Coulomb electrostatics. Finally, a long-range dispersion correction term was added to both energy and pressure.

Table S2: Lennard-Jones parameters, point charges and atomic masses.

Site	Mass (a.u)	q (a.u.)	σ (nm)	ε (kJ mol^{-1})
Ow	15.9994	-0.8476	0.31656	0.65019
Hw	1.0080	0.4238	0.0	0.0
N	14.0067	-0.900	0.330	0.711280
Nc	14.0067	-0.300	0.3250	0.711280
Nt	14.0067	0.000	0.3250	0.711280
Cn	12.0110	0.060	0.350	0.276144
Cnc	12.0110	0.190	0.350	0.276144
C	12.0110	-0.120	0.350	0.2761444
C3	12.0110	-0.180	0.350	0.2761444
Ct	12.0110	0.130	0.350	0.2761444
Hc	1.0080	0.060	0.250	0.125520
Hn	1.0080	0.360	0.0	0.0
Hnc	1.0080	0.330	0.0	0.0
Hcn	1.0080	0.060	0.250	0.06276
SiN	28.0855	1.3292	0.4435	0.39748
Cl	35.4530	-1.0	0.441724	0.492833
SiI	28.0855	1.0801	0.4435	0.39748
OhN	15.9994	-0.7641	0.34618	0.665674
OhI	15.9994	-0.7481	0.34618	0.665674
HoN	1.0080	0.4318	0.23541	0.413379
HoI	1.0080	0.3684	0.23541	0.413379
Oc	15.9994	-0.9410	0.34618	0.665674
ONN	15.9994	-0.6646	0.34506	0.67864
OII	15.9994	-0.7594	0.34506	0.67864
OIN	15.9994	-0.7120	0.34506	0.67864

Table S3: Bond lengths.

Bond	Lenght (nm)
Ow-Hw	0.100
N-Hn	0.101
N-Cn	0.1448
Nc-Hcn	0.101
Nc-Cnc	0.1471
Nt-Ct	0.1471
Cn-Hcn	0.109
Cn-C	0.1529
Cnc-Hc	0.109
Cnc-C	0.1529
C-Hc	0.109
C-C	0.1529
C3-C	0.1529
C3-Hc	0.1529
Ct-Hc	0.109
SiN-OhN	0.1652
SiI-OhI	0.1695
SiI-Oc	0.1581
SiN-ONN	0.1651
SiN-OIN	0.1651
SiI-OII	0.169
SiI-OIN	0.169
OhN-HoN	0.0968
OhI-HoI	0.0968

Table S4: Bond angles and harmonic force constants.

Angle	θ_0 (deg)	k_θ (kJ mol^{-1} rad^{-2})
Hw-Ow-Hw	109.47	—
Hn-N-Hn	106.4	364.845
Hn-N-Cn	109.5	292.880
Hnc-Nc-Hnc	109.5	292.880
Hnc-Nc-Cnc	109.5	292.880
N-Cn-C	109.47	470.281
N-Cn-Hcn	109.5	292.880
Nc-Cnc-C	111.2	669.44
Nc-Cnc-Hcn	109.5	292.800
Nt-Ct-Hc	109.5	292.880
Hcn-Cn-Hcn	107.8	276.144
Hcn-Cn-C	110.7	313.800
Hcn-Cnc-Hcn	107.8	276.144
Hcn-Cnc-C	110.7	313.800
Cn-C-C	112.7	488.273
Cn-C-Hc	110.7	313.800
Cnc-C-C	112.7	488.273
Cnc-C-Hc	110.7	313.800
Ct-Nt-Ct	113.0	418.400
Hc-C-C	110.7	313.800
C3-C-Hc	110.7	313.800
C-C3-HC	110.7	313.800
Hc-C-Hc	107.8	276.144
Hc-C3-Hc	107.8	276.144
Hc-Ct-Hc	107.8	276.144
C-C-C	112.7	488.273
SiN-OhN-HoN	118.0442	109.29
SiI-OhI-HoI	118.0442	109.29
OhN-SiN-OhN	116.2621	255.64
OhI-SiI-OhI	116.2621	255.64
OhI-SiI-Oc	166.2621	255.64
SiN-ONN-SiN	174.2152	19.52
SiN-OIN-SiI	174.2152	19.52
SiI-OII-SiI	174.2152	19.52
OhN-SiN-ONN	111.0860	7343.28
OhN-SiN-OIN	111.0860	7343.28
OhI-SiI-OIN	111.0860	7343.28
OhI-SiI-OII	111.0860	7343.28
Oc-SiI-OIN	111.0860	7343.28
Oc-SiI-OII	111.0860	7343.28

Table S5: Dihedral torsion parameters.

Dihedral	C_0 (kJ mol^{-1})	C_1 (kJ mol^{-1})	C_2 (kJ mol^{-1})	C_3 (kJ mol^{-1})	C_4 (kJ mol^{-1})	C_5 (kJ mol^{-1})
Hn-N-Cn-Hcn	0.83680	2.51040	0.0	-3.34720	0.0	0.0
Hn-N-Cn-C	-1.26775	3.02085	1.74473	-3.49782	0.0	0.0
Hnc-Nc-Cnc-Hcn	0.54601	1.63803	0.0	-2.18405	0.0	0.0
Hnc-Nc-Cnc-C	-1.26775	3.02085	1.74473	-3.49782	0.0	0.0
N-Cn-C-Hc	-4.09614	5.08775	2.96645	-3.95806	0.0	0.0
N-Cn-C-C	3.33465	-1.5526	2.82001	-4.60240	0.0	0.0
Nc-Cnc-C-C	5.77183	-2.67148	0.95814	-4.05848	0.0	0.0
Nc-Cnc-C-Hc	0.8033	2.4099	0.0	-3.21331	0.0	0.0
Hcn-Cn-C-Hc	0.62760	1.88280	0.0	-2.51040	0.0	0.0
Hcn-Cn-C-C	0.62760	1.88280	0.0	-2.51040	0.0	0.0
Hcn-Cnc-C-Hc	0.62760	1.88280	0.0	-2.51040	0.0	0.0
Hc-C-C-Hc	0.62760	1.88280	0.0	-2.51040	0.0	0.0
Hc-C-C3-Hc	0.62760	1.88280	0.0	-2.51040	0.0	0.0
Hcn-Cnc-C-C	0.62760	1.88280	0.0	-2.51040	0.0	0.0
Hc-Ct-Nt-Ct	0.63179	1.89535	0.0	-2.52714	0.0	0.0
Cn-C-C-C	2.92880	-1.46440	0.20920	-1.67360	0.0	0.0
Cnc-C-C-C	2.92880	-1.46440	0.20920	-1.67360	0.0	0.0
C-C-C-C	2.92880	-1.46440	0.20920	-1.67360	0.0	0.0
OhN-SiN-OhN-HoN	14.8473	9.1554	-3.6233	2.0686	0.0	0.0
OhI-SiI-OhI-HoI	14.8473	9.1554	-3.6233	2.0686	0.0	0.0
Oc-SiI-OhI-HoI	14.8473	9.1554	-3.6233	2.0686	0.0	0.0
ONN-SiN-OhN-HoN	15.2038	23.8622	-2.5673	-9.8910	0.0	0.0
OIN-SiN-OhN-HoN	15.2038	23.8622	-2.5673	-9.8910	0.0	0.0
OII-SiI-OhI-HoI	15.2038	23.8622	-2.5673	-9.8910	0.0	0.0
OIN-SiI-OhI-HoI	15.2038	23.8622	-2.5673	-9.8910	0.0	0.0
OhN-SiN-ONN-SiN	-3.3698	-4.0041	-0.6343	0.0	0.0	0.0
OhN-SiN-OIN-SiI	-3.3698	-4.0041	-0.6343	0.0	0.0	0.0
OhI-SiI-OII-SiI	-3.3698	-4.0041	-0.6343	0.0	0.0	0.0
OhI-SiI-OIN-SiN	-3.3698	-4.0041	-0.6343	0.0	0.0	0.0
Oc-SiI-OII-SiI	-3.3698	-4.0041	-0.6343	0.0	0.0	0.0
Oc-SiI-OIN-SiN	-3.3698	-4.0041	-0.6343	0.0	0.0	0.0

Initial configurations for all-atom (AA) simulations were created by placing in the center of the simulation box a preformed micelle consisting of 70 surfactants (charged or neutral). The preformed micelle was made using the software Packmol[10] and its size chosen to match, approximately, the experimentally measured aggregation number for the system, in the absence of silica, at 50 °C[11]. In the next step, counter-ions, i.e. chloride (Cl^-) and tetramethylammonium (TMA^+), as well as silica monomers and dimers were randomly added to

the box and the system solvated with a fixed number of water molecules. The original reacting mixture for HMS materials contains also ethanol, however, to reduce the complexity of the simulations this was neglected and replaced by water, as done previously in modelling the synthesis of MCM-41[6,12,13]. All atomistic simulations performed are listed in Table S6, however it should be noted that only the systems marked with an asterisk have been presented and discussed explicitly in the main body of this work. The remainder have also been included since they were used to develop the CG model, as will be later discussed in Section 3 of this document.

Table S6: Number of molecules in each atomistic MD simulation of preformed aggregates used to develop parameters of the coarse-grained model. Only simulations marked with (*) are discussed in the main body of this work. DDA^+, charged surfactant; DDA, neutral surfactant; Cl^-, chloride ion; TMA^+, tetramethylammonium ion; SI, anionic silica monomer; SN, neutral silica monomer; SISI, silica dimer with two charges; SISN, silica dimer with one charge; SNSN, neutral silica dimer, and water. The final box size is approximately 8.1 nm in all directions.

System	DDA^+	DDA	Cl^-	TMA^+	SI	SN	SISI	SISN	SNSN	water
(*) AA-DDA^+	70		70							16420
AA-DDA^+/SI	70				70					16420
AA-DDA^+/SN	70		70			70				16420
(*) AA-DDA^+/SI/SN	70				70	70				16420
AA-DDA^+/SISI	70						35			16420
AA-DDA^+/SISN	70		35					35		16420
AA-DDA^+/SNSN	70		70						35	16420
AA-DDA		70								16420
(*) AA-DDA/SN		70				70				16420
AA-DDA/SI		70		70	70					16420
AA-DDA/SN/SI		70		70	70	70				16420

For each AA system studied, an energy minimisation step followed by two short equilibration steps (first *NVT* and then *NPT*) were performed. Then, the system was run for production at 323 K in the *NPT* ensemble for at least 10 ns. The temperature was kept constant using the Nosé-Hoover thermostat[14] and the pressure fixed at 1 bar employing the Parrinello-Rahman barostat[15]. The equations of motion were integrated using the leap-frog algorithm[16] with a time step of 2 fs. The simulation boxes were always cubic with periodic

boundary conditions applied in x, y and z directions.

3 Coarse-grained simulations

Two types of coarse-grained (CG) simulations were considered: i) simulations of small systems consisting of preformed micelles in solution with counter-ions and/or silicates, used to develop and validate the CG interaction parameters and ii) simulations of large systems starting from random distributions of all species in solution, used to investigate the mechanism of formation of HMS materials.

CG model development The small systems, used to develop our CG model, were created similarly to the atomistic ones by placing a preformed micelle of CG surfactants in the center of a simulation box of approximately 8 nm (see Table S7). In the next step, all other species were added and the system solvated with a pre-equilibrated box of CG water. The number of CG water beads used in each system was adjusted to match the concentration of the corresponding AA simulation, taking into account that in the MARTINI force field[17] a CG chloride ion includes its solvation shell (made of 6 atomistic water molecules), and that a single water bead corresponds to 4 atomistic water molecules. Another feature of the MARTINI model for water is that it tends to undergo freezing at ambient temperature, so it is normally recommended to replace 10 % of the water with so-called antifreeze (AF) particles (BP_4 type beads) to avoid this issue. With regard to this work, no antifreeze particles were included since the temperature used in our simulations (50 °C) is considerably above the freezing temperature of the MARTINI model for water.

The approach used to develop our CG parameters is based on the methodology employed by Pérez-Sánchez et al. to obtain their CG model of MCM-41 formation[18]. This involved comparing density profiles of preformed aggregates of the same size obtained from AA and CG simulations, and subsequently tuning such interactions at the CG level until the best set of parameters reproducing the AA results was found[18]. Specifically, the final set of

Table S7: Number of molecules in each coarse-grained MD simulation of preformed aggregates used to develop parameters of the coarse-grained model. DDA^+, charged surfactant; DDA, neutral surfactant; Cl^-, chloride ion; TMA^+, tetramethylammonium ion; SI, anionic silica monomer; SN, neutral silica monomer; SISI, silica dimer with two charges; SISN, silica dimer with one charge; SNSN, neutral silica dimer, and water. The final box size is approximately 8.1 nm in all directions.

System	DDA^+	DDA	Cl^-	TMA^+	SI	SN	SISI	SISN	SNSN	water
AA-DDA^+	70		70							4000
AA-DDA^+/SI	70				70					4105
AA-DDA^+/SN	70		70			70				4000
AA-DDA^+/SI/SN	70				70	70				4105
AA-DDA^+/SISI	70						35			4105
AA-DDA^+/SISN	70		35					35		4053
AA-DDA^+/SNSN	70		70						35	4000
AA-DDA		70								4105
AA-DDA/SN		70				70				4105
AA-DDA/SI		70		70	70					4105
AA-DDA/SN/SI		70		70	70	70				4105

parameters was obtained in a progressive manner by gradually including more species into our simulations, hence allowing, at each step, to validate the previously obtained parameters.

Prior to the production runs, the CG systems were energy minimised, followed by a short relaxation step. Production simulations were then performed in the *NPT* ensemble for up to 40 ns by keeping the temperature constant at 323 K using the velocity-rescaling thermostat[19] and the pressure fixed at 1 bar using the Parrinello-Rahman barostat[15]. The equations of motion were integrated using the the leap-frog algorithm[16] with a time step of 40 fs, and cubic periodic boundary conditions were applied in all directions.

Trajectories were then analysed using an adaptation of the Hoshen-Kopelman cluster-counting algorithm[20]. For this purpose, two surfactant molecules were considered part of the same cluster if, at the atomistic level, the distance between the last four atoms (one carbon and three hydrogens), or, at coarse-grained level, the distance between the last tail beads, was less than 0.75 nm. This value was chosen since it is close to the position of the first minimum in the respective radial distribution functions. The equation used to compute

the number-average cluster size for clusters larger than 4 molecules is:

$$< CN_N >_4 = \frac{\sum_{n=4}^{\infty} n[M_n]}{\sum_{n=4}^{\infty} [M_n]} \quad (1)$$

where n indicates the size of the clusters and M_n the concentration of clusters with n molecules. The cluster-counting algorithm allowed us to calculate AA and CG average density profiles, measured from the micelle centre of mass (COM). It should be noted that the standard mass of a MARTINI bead is 72 a.u.; however, for the purpose of the density profile calculation, real masses were attributed to each bead to match the corresponding atomistic group (i.e. head, tail, monomer, dimers, etc.). For example the mass of the bead representing the charged head is approximately 17 a.u. (i.e. the mass of one nitrogen and three hydrogens), while the mass of the SN bead is approximately 96 a.u. (i.e. the mass of one silicon atom, four oxygens and four hydrogens), etc.. Figure S5 displays a schematic representation of the mapping scheme adopted for each species considered.

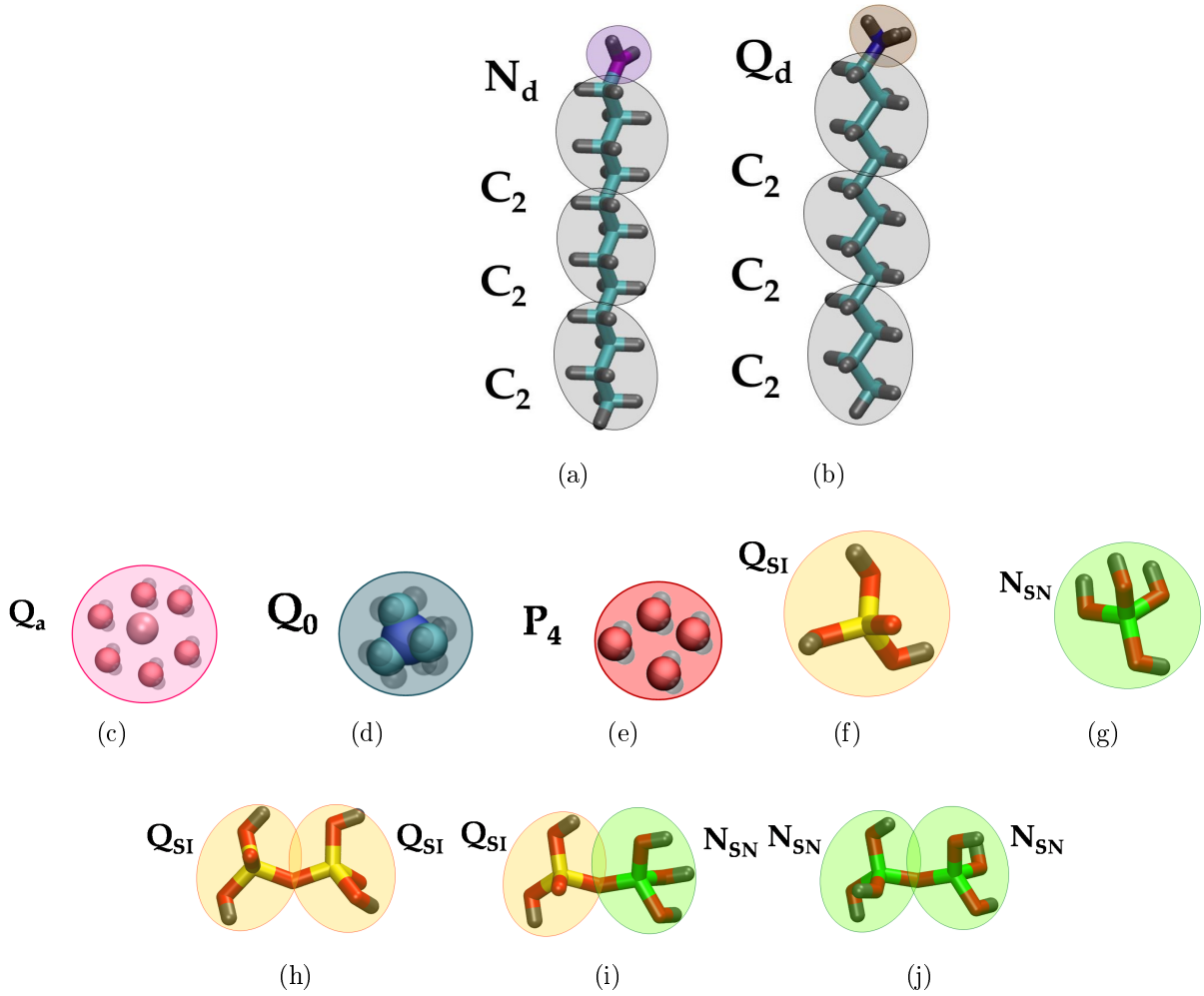

Figure S5: Schematic representation of the CG mapping schemes adopted in this work. DDA surfactant, (a); DDA^+, (b); solvated chloride counter-ions, (c); TMA^+ counter-ions, (d); water, (e); anionic silica monomer, (f); neutral silica monomer, (g); doubly deprotonated dimer, (h); singly deprotonated dimer, (i) and neutral dimer, (j).

In the following, CG density profiles and representative snapshots obtained by employing this methodology are presented in comparison to the corresponding AA systems (see Figures S6-S14).

In order to improve structural agreement between AA and CG micelle density profiles, a higher angle force constant than the standard MARTINI value (50 $kJ\,mol^{-1}$ instead of 25 $kJ\,mol^{-1}$) was used to model surfactant beads, charged or neutral. This was shown to produce narrower surfactant head profiles as well as steeper tail and water distributions. It

should be noted that higher values of the angle force constant (up to $f = 500$ kJ mol^{-1}) were also tested producing even better agreement with AA results. However, when these very high angle force constant values were employed to model large systems at high surfactant concentration, freezing was observed to take place due to the extreme rigidity of the model. We attribute the discrepancies between AA and CG profiles for chloride counter-ions (pink curves in Figure S6, Figure S13 and Figure S14) to the larger size of the ion at CG level. In fact, by including also a solvation shell, in the CG bead, chloride ions are not allowed to adsorb as close to the surfactant heads as they do at atomistic level. Furthermore, neutral micelles appear to be more disordered than charged ones: some of the head groups are located inside the micelle core and some water molecules can penetrate inside it (see Figure S7). Since neutral DDA surfactants cannot dissolve in pure water[21], the presence of head groups in the core of the neutral micelles is an indication that, at these conditions, micelles are not the thermodynamically stable aggregation state (see Figure 2-b of the main paper). Nevertheless, also in this regard, AA and CG models show the same qualitative behaviour.

For the system containing silica monomers and dimers, we notice that although the height of the density peaks is not exactly captured by the CG model, the position and width of both silica and head group peaks is in general matched quite well with the AA profiles. We attribute the small discrepancies between CG and AA profiles to the more disordered nature of CG surfactant micelles, brought about by the lower resolution of the model.

The final set of CG parameters is summarised in Table S8.

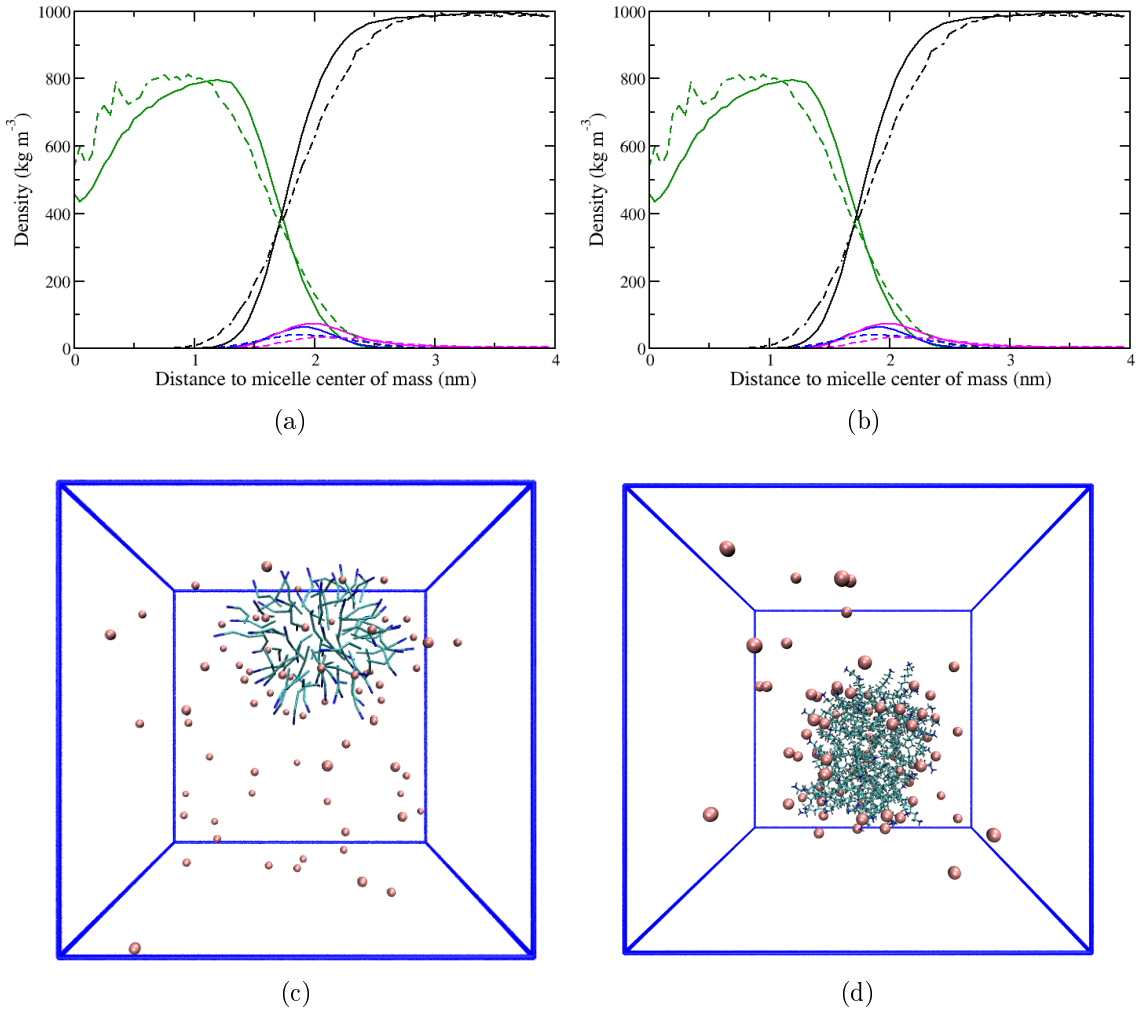

Figure S6: Top: (a)-(b), Comparison between atomistic (solid lines) and coarse-grained (dashed lines) average micelle density profiles obtained for the reference system with DDA^+ surfactants and Cl^- ions. The angle force constant is set to $f = 50\,\mathrm{kJ\,mol^{-1}}$ the CG surfactant. Tails, dark green; charged heads, blue; chloride ions, pink and water, black. Bottom: (c)-(d), Snapshots comparing the final configurations obtained with coarse-grained (c) and atomistic (d) simulations for the same system. Colour code for the CG snapshot is: charged heads, blue and tails, teal. Colour code for the AA snapshot is: charged nitrogens, blue; carbons, teal; hydrogens, grey and chloride ions, pink. Water has been removed for clarity.

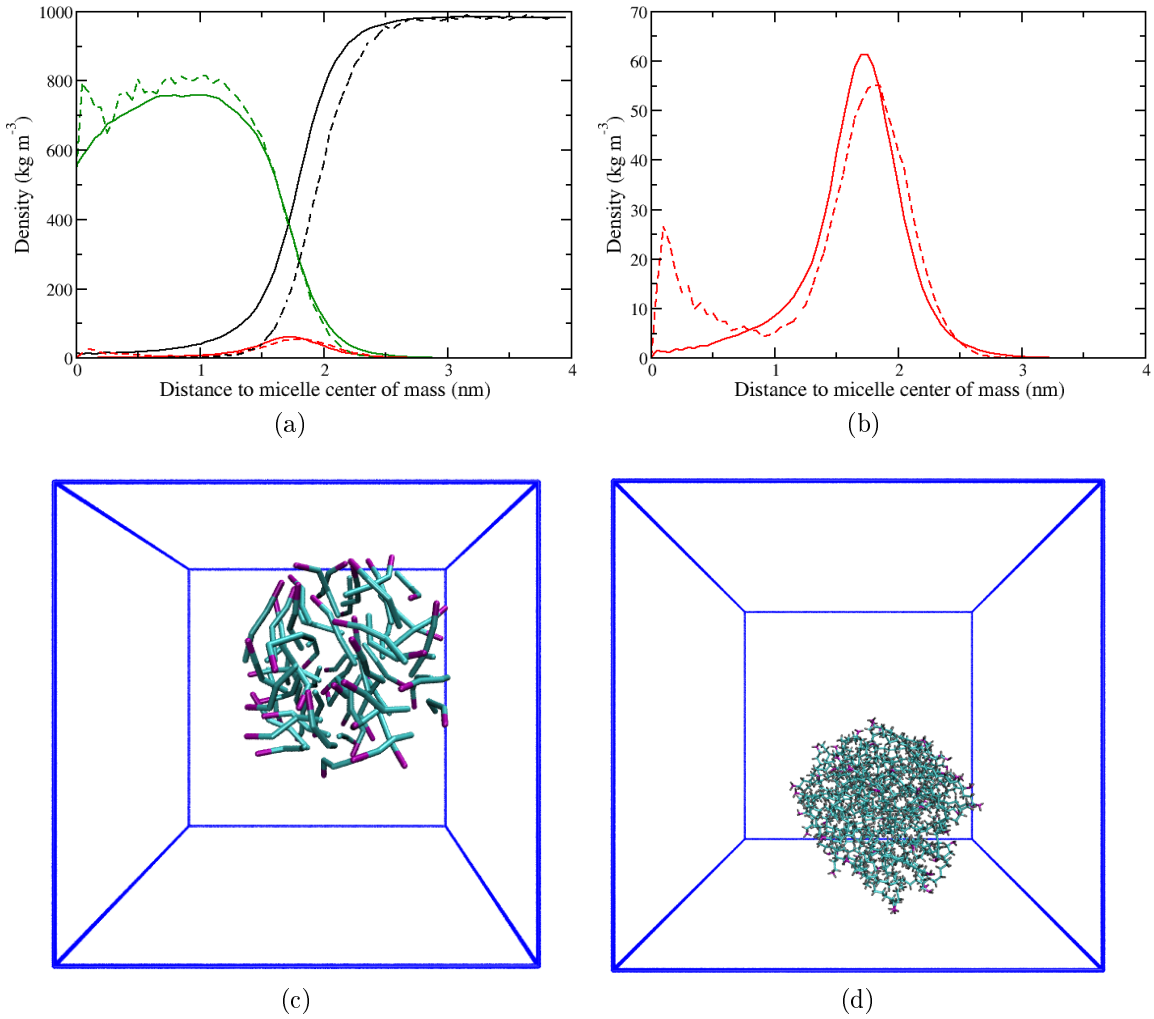

Figure S7: Top: (a)-(b), Comparison between atomistic (solid lines) and coarse-grained (dashed lines) average micelle density profiles obtained for the reference system with DDA surfactants. The angle force constant is set to $f = 50$ kJ mol^{-1} the CG surfactant. Tails, dark green; neutral heads, red and water, black. Bottom: (c)-(d), Snapshots comparing the final configurations obtained with coarse-grained (c) and atomistic (d) simulations for the same system. Colour code for the CG snapshot is: neutral heads, purple and tails, teal. Colour code for the AA snapshot is: neutral nitrogens, purple; carbons, teal and hydrogens, grey. Water has been removed for clarity.

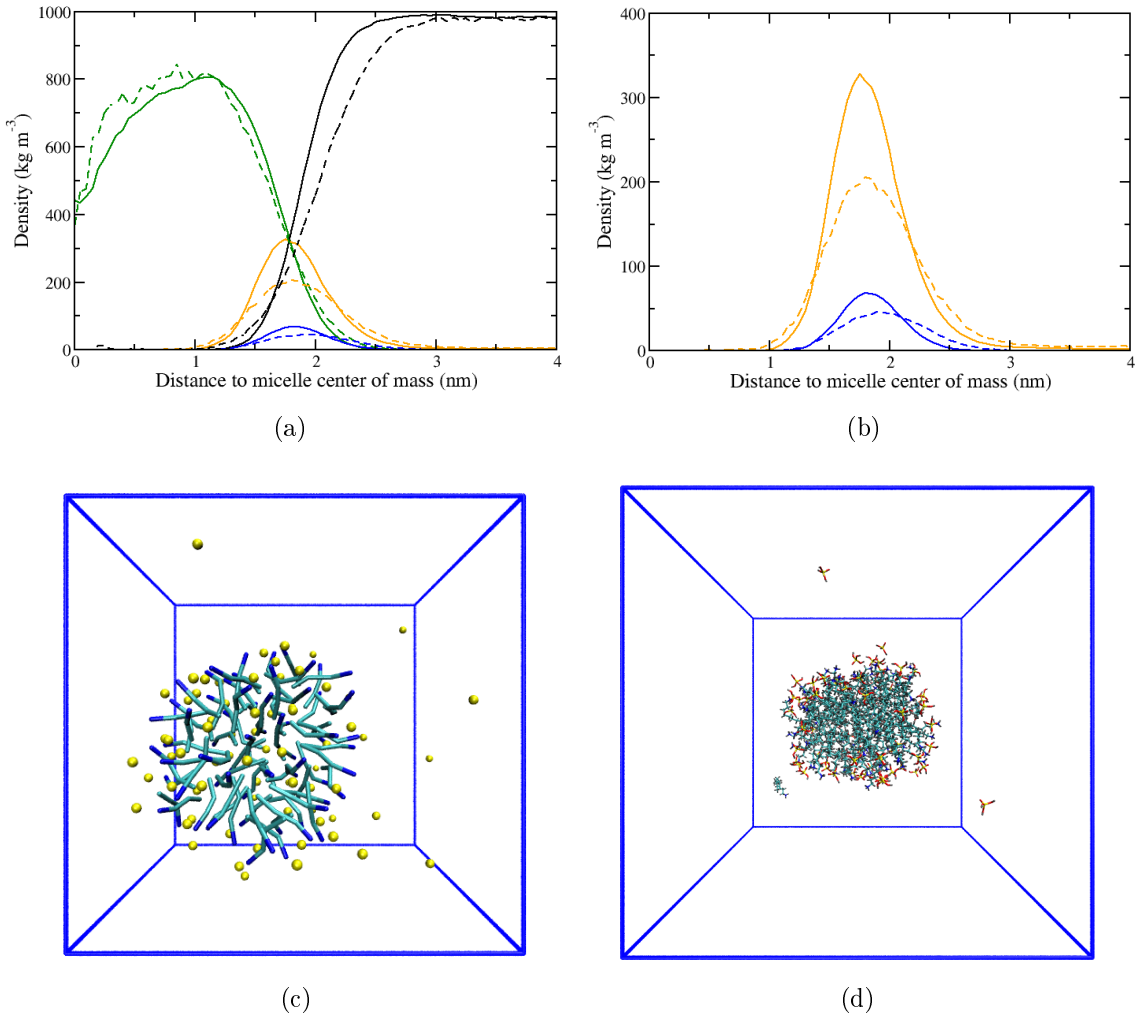

Figure S8: Top: (a)-(b), Comparison between atomistic (solid lines) and coarse-grained (dashed lines) average micelle density profiles obtained for the system containing DDA^+ surfactants and SI monomers (Q_{SI}-Q_d = II). Tails, dark green; charged heads, blue; anionic silica monomers, yellow and water, black. Bottom: (c)-(d), Snapshots comparing the final configurations obtained with coarse-grained (c) and atomistic (d) simulations for the same system. Colour code for the CG snapshot is: charged heads, blue; tails, teal and SI monomers, yellow. Colour code for the AA snapshot is: charged nitrogens, blue, carbons, teal, hydrogens, grey; oxygens, red and charged silicons, yellow. Water has been removed for clarity.

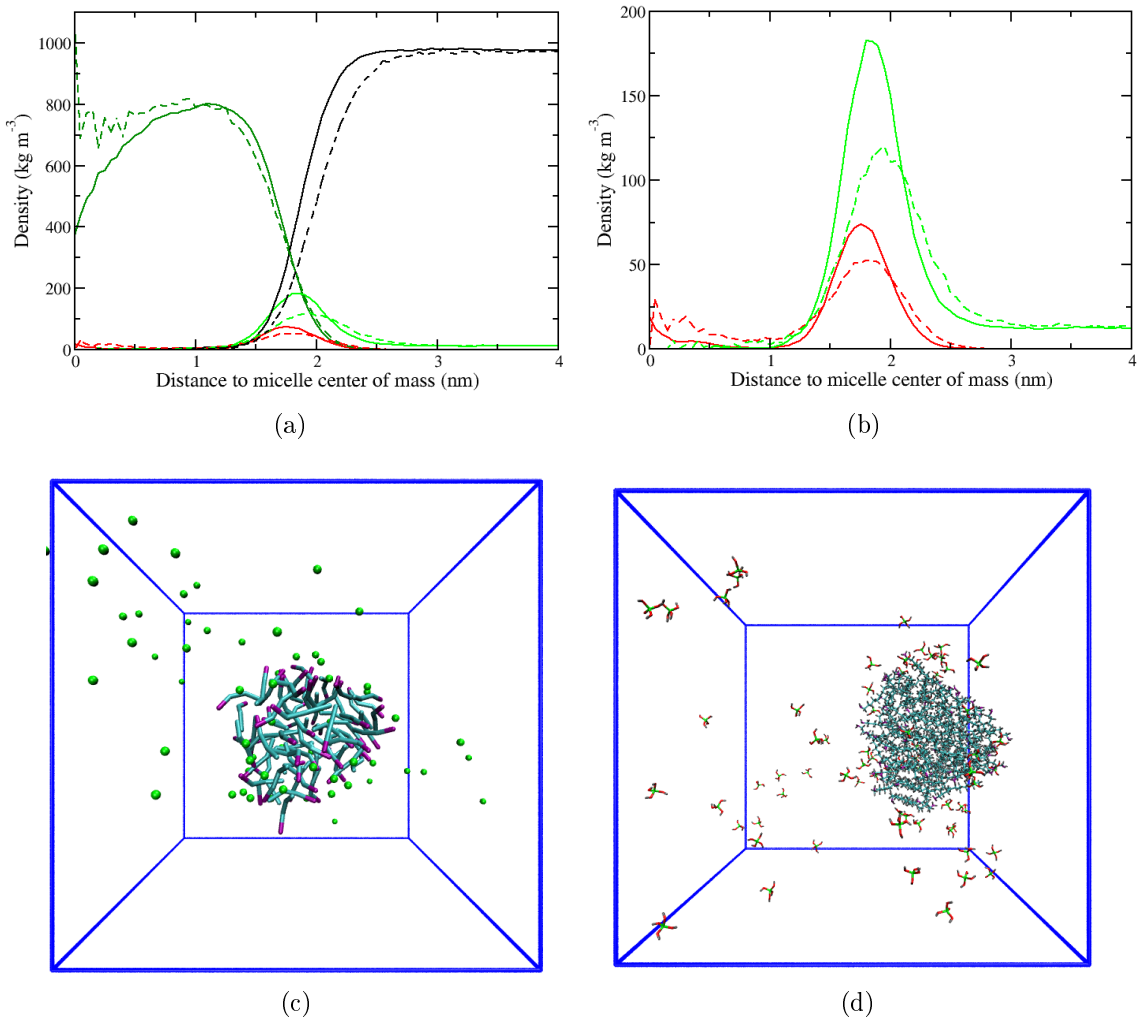

Figure S9: Top: (a)-(b), Comparison between atomistic (solid lines) and coarse-grained (dashed lines) average micelle density profiles obtained for the system containing DDA surfactants and SN monomers (N_{SN}-$N_d = 0$). Tails, dark green; neutral heads, red; neutral silica monomers, green and water, black. Bottom: (c)-(d), Snapshots comparing the final configurations obtained with coarse-grained (c) and atomistic (d) simulations for the same system. Colour code for the CG snapshot is: neutral heads, purple; tails, teal and SN monomers is green. Colour code for the AA snapshot is: neutral nitrogens, purple; carbons, teal; hydrogens, grey; oxygens, red and neutral silicons, green. Water has been removed for clarity.

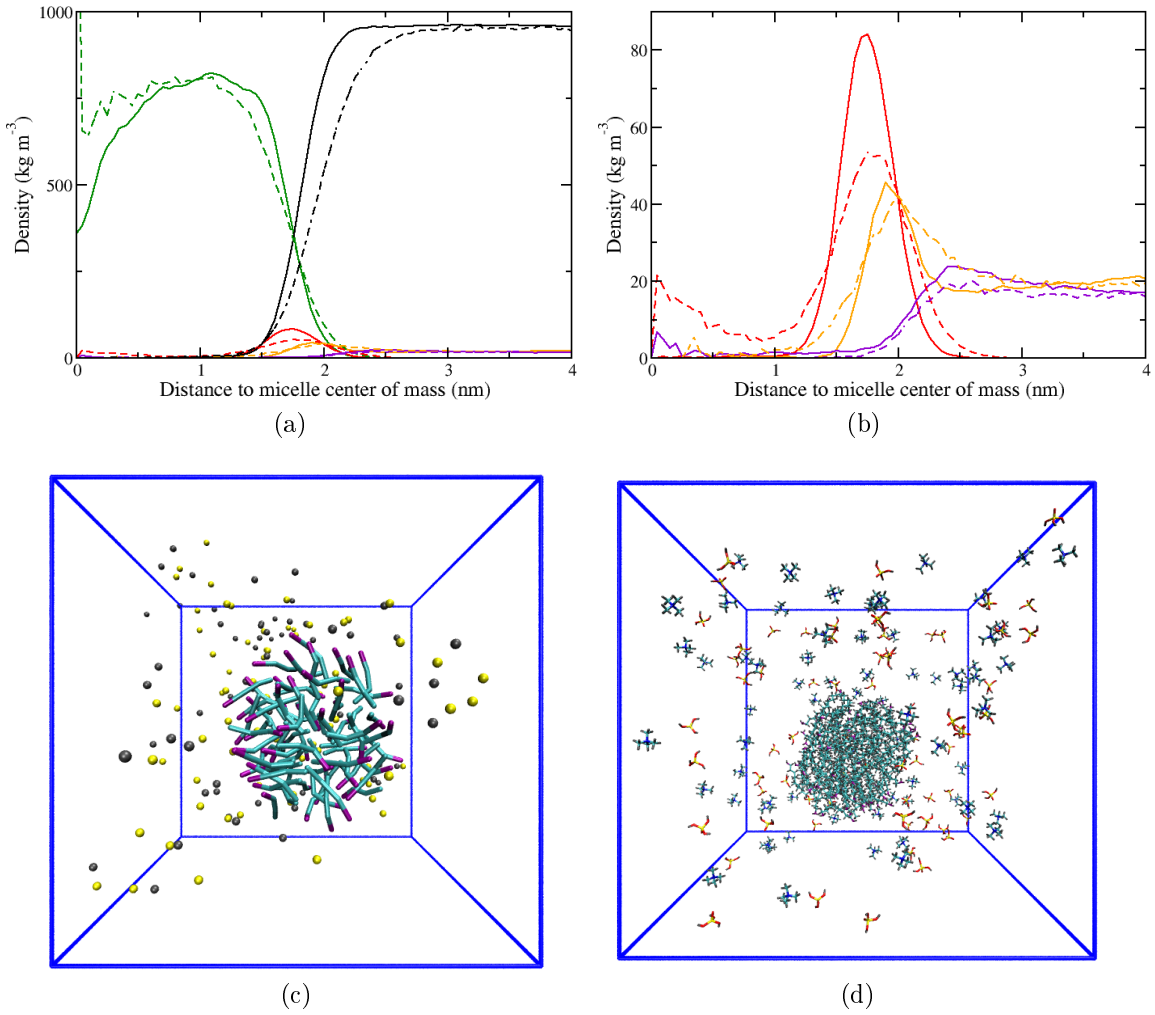

Figure S10: Top: (a)-(b), Comparison between atomistic (solid lines) and coarse-grained (dashed lines) average micelle density profiles obtained for the system containing DDA surfactants, SI monomers and TMA counter-ions (Q_{SI}-N_d = III). Tails, dark green; neutral heads, red; anionic silica monomers, yellow; TMA counter-ions, purple and water, black. Bottom: (c)-(d), Snapshots comparing the final configurations obtained with coarse-grained (c) and atomistic (d) simulations for the same system. Colour code for the CG snapshot is: neutral heads, purple; tails, teal; SI monomers, yellow and TMA counter-ions grey. Colour code for the AA snapshot is: neutral nitrogens, purple, carbons, teal, hydrogens, grey; oxygens, red and charged silicons, yellow. Water has been removed for clarity. Water has been removed for clarity.

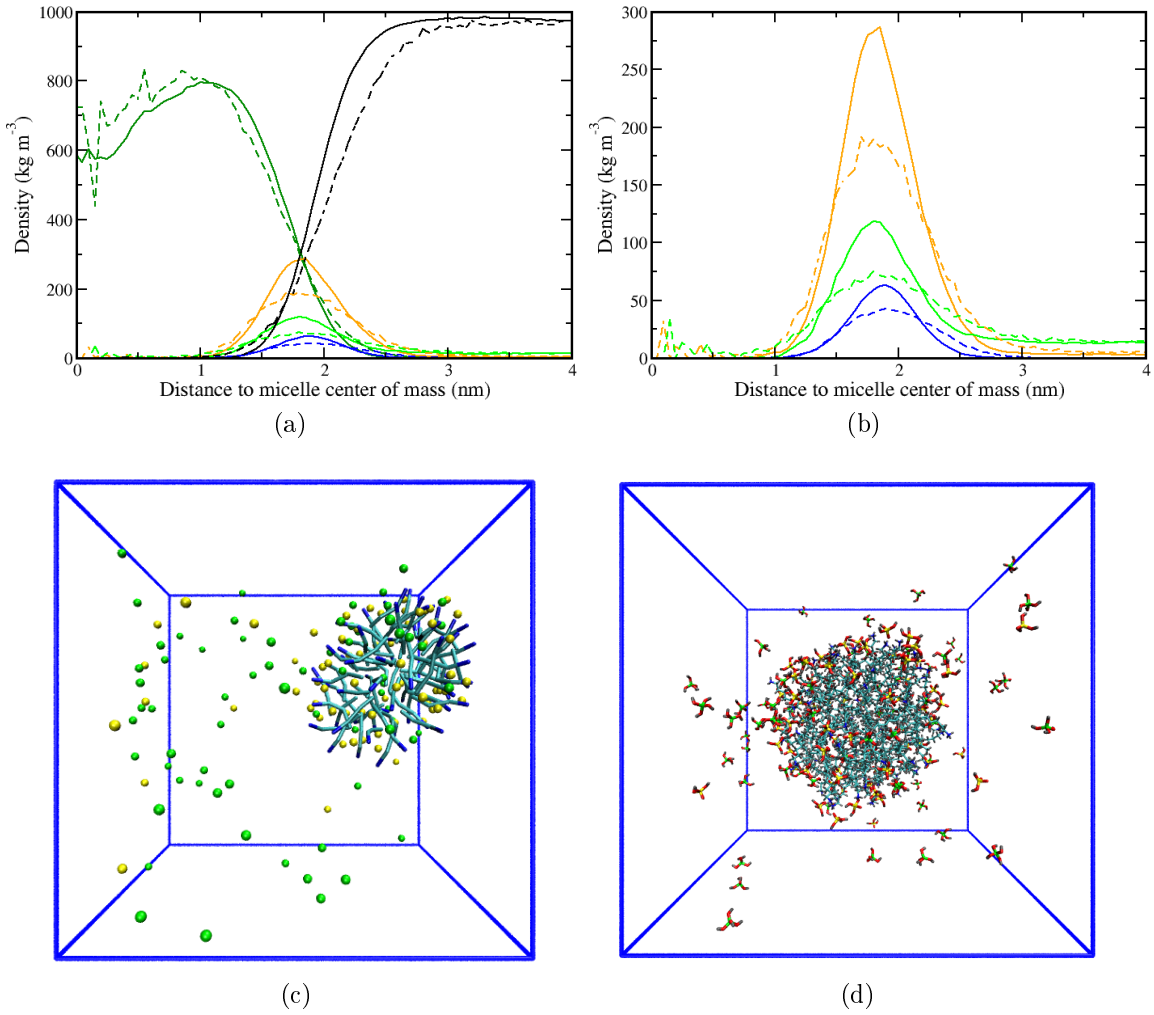

Figure S11: Top: (a)-(b), Comparison between atomistic (solid lines) and coarse-grained (dashed lines) average micelle density profiles obtained for the system containing DDA^+ surfactants and both SI and SN monomers (Q_{SI}-$N_{SN} = 0$ and N_{SN}-$Q_d = 0$). Tails, dark green; charged heads, blue; anionic silica monomers, yellow; neutral silica monomers, green and water, black. Bottom: (c)-(d), Snapshots comparing the final configurations obtained with coarse-grained (c) and atomistic (d) simulations for the same system. Colour code for the CG snapshot is: charged heads, blue; tails, teal; SI monomers, yellow and SN monomers is green. Colour code for the AA snapshot is: charged nitrogens, blue, carbons, teal, hydrogens, grey; oxygens, red; charged silicons, yellow and neutral silicons, green. Water has been removed for clarity.

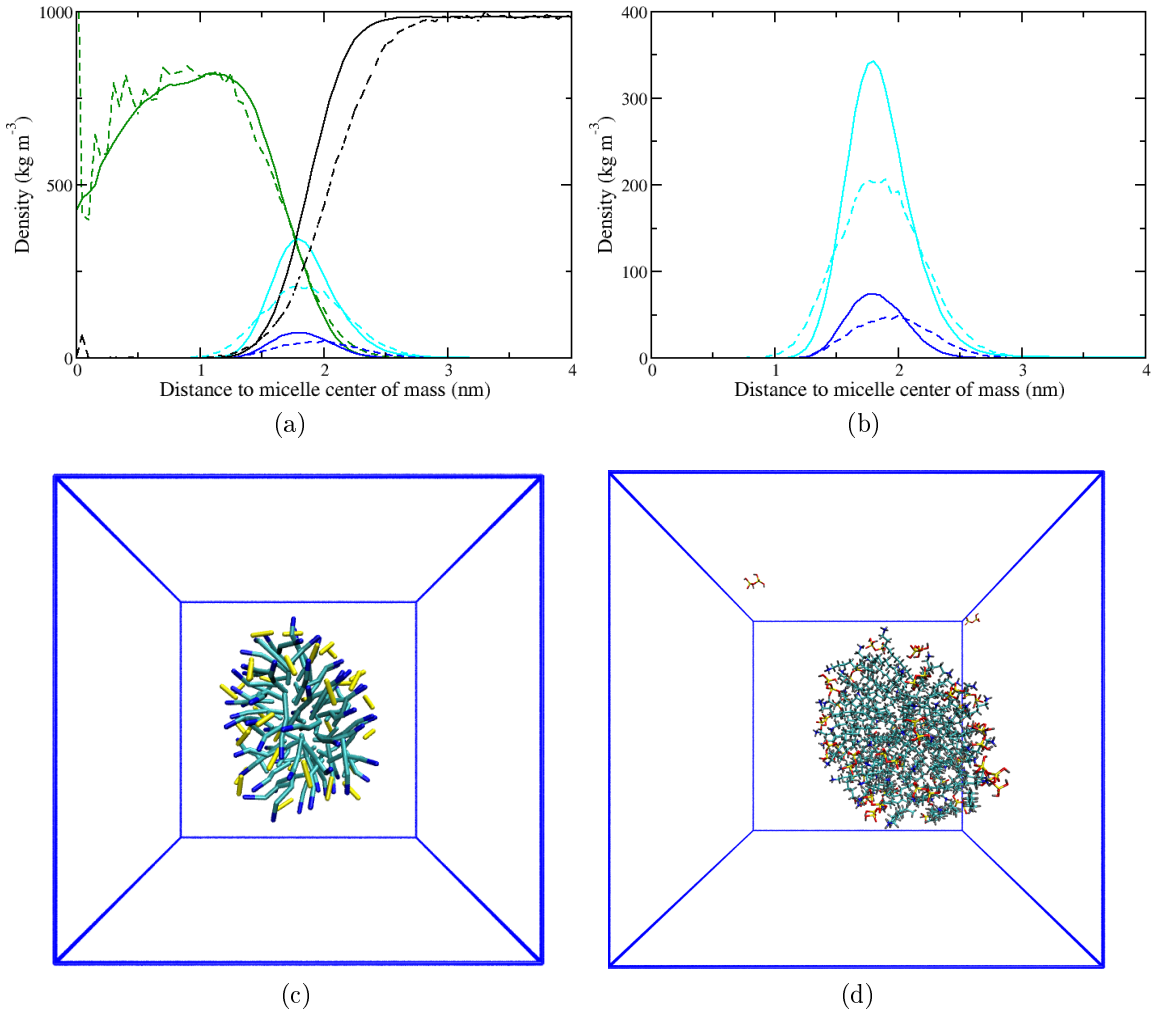

Figure S12: Top: (a)-(b), Comparison between atomistic (solid lines) and coarse-grained (dashed lines) average micelle density profiles obtained for the system containing DDA^+ surfactants and SISI dimers. The SISI dimer is represented by two Q_{SI} beads. Tails, dark green; charged heads, blue; SISI dimers, cyan and water, black. Bottom: (c)-(d), Snapshots comparing the final configurations obtained with coarse-grained (c) and atomistic (d) simulations for the same system. Colour code for the CG snapshot is: charged heads, blue; tails, teal and SISI dimers, yellow. Colour code for the AA snapshot is: charged nitrogens, blue; carbons, teal; hydrogens, grey; oxygens, red and charged silicons, yellow. Water has been removed for clarity.

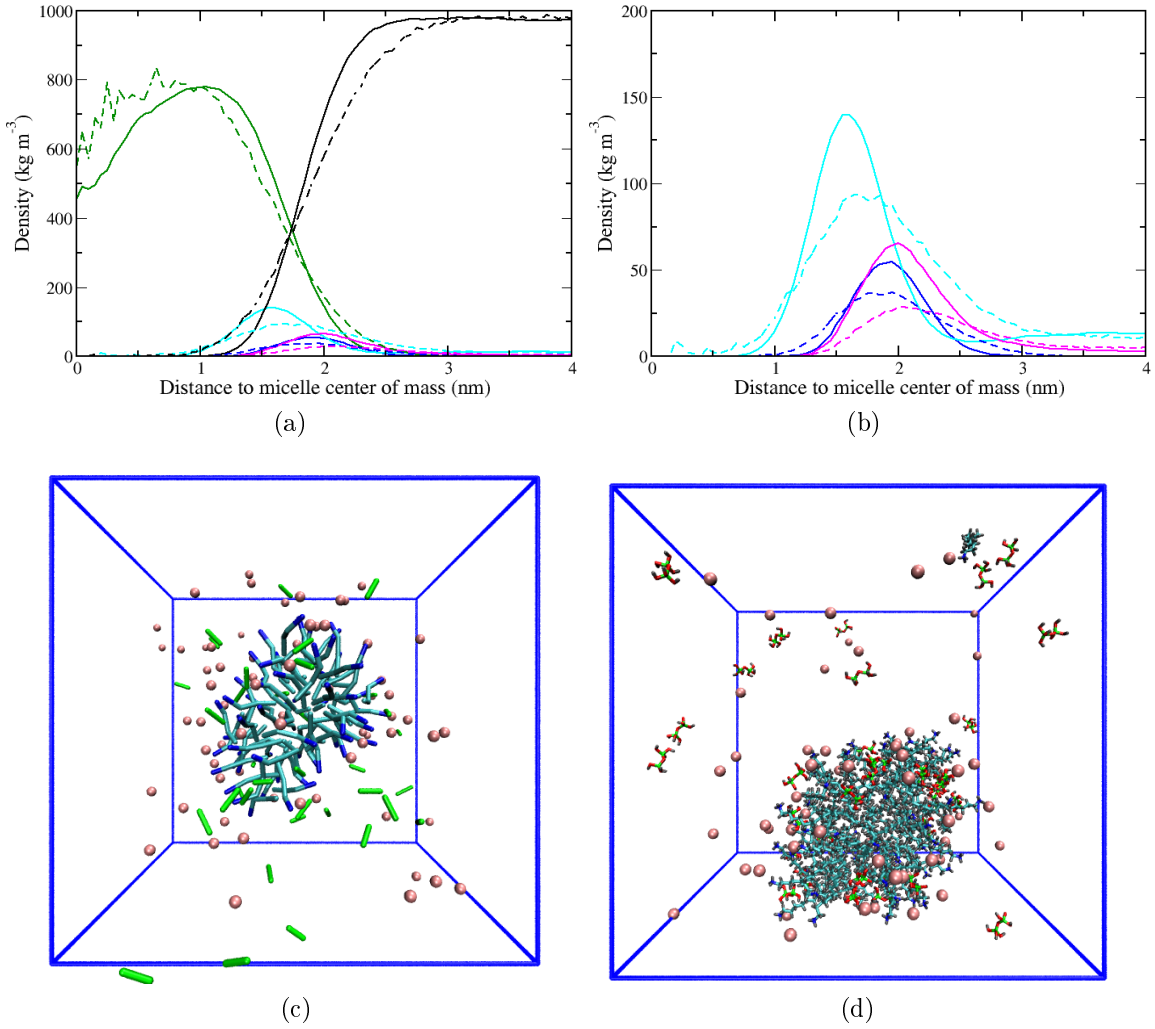

Figure S13: Top: (a)-(b), Comparison between atomistic (solid lines) and coarse-grained (dashed lines) average micelle density profiles obtained for the system containing DDA^+ surfactants, SNSN dimers and Cl ions. The SNSN dimer is represented by two N_{SN} beads. Tails, dark green; charged heads, blue; SNSN dimers, cyan; chloride ion, purple and water, black. Bottom: (c)-(d), Snapshots comparing the final configurations obtained with coarse-grained (c) and atomistic (d) simulations for the same system. Colour code for the CG snapshot is: charged heads, blue; tails, teal, SNSN dimers, green and Cl ions, pink. Colour code for the AA snapshot is: charged nitrogens, blue, carbons, teal, hydrogens, grey; oxygens, red and neutral silicons, green. Water has been removed for clarity.

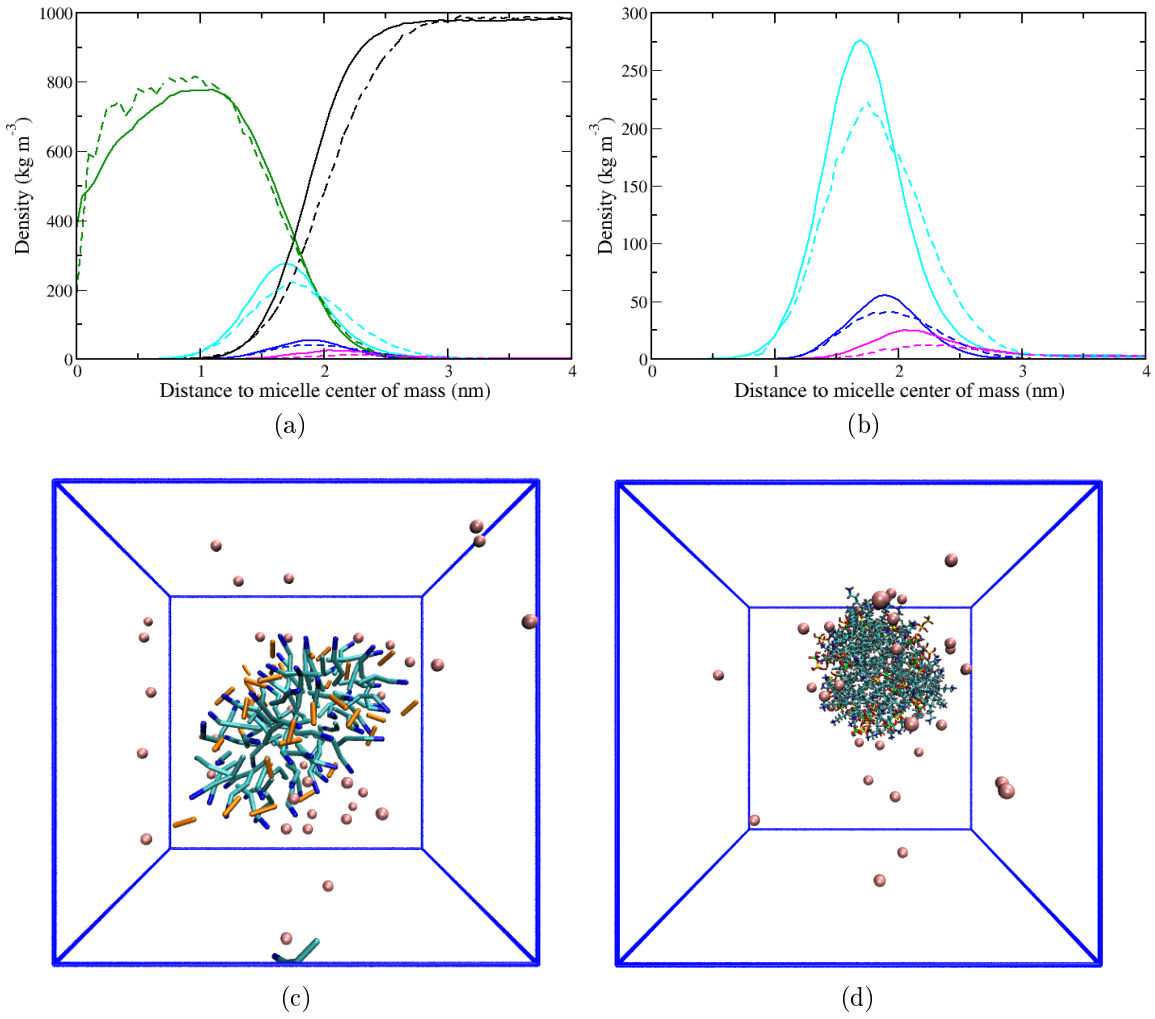

Figure S14: Top: (a)-(b), Comparison between atomistic (solid lines) and coarse-grained (dashed lines) average micelle density profiles obtained for the system containing DDA^+ surfactants, SISN dimers and Cl ions. The SISN dimer is represented by one Q_{SI} and one N_{SN} beads. Tails, dark green; charged heads, blue; SISN dimers, cyan; chloride ion, purple and water, black. Bottom: (c)-(d), Snapshots comparing the final configurations obtained with coarse-grained (c) and atomistic (d) simulations for the same system. Colour code for the CG snapshot is: charged heads, blue; tails, teal, SISN dimers, orange and Cl ions, pink. Colour code for the AA snapshot is: charged nitrogens, blue; carbons, teal; hydrogens, grey; oxygens, red; charged silicons, yellow and neutral silicons, green. Water has been removed for clarity.

Table S8: Interaction matrix for CG beads used in this work. The notation follows the original MARTINI paper[17]: 0 - *supra attractive* ($\epsilon = 5.6$ kJ mol^{-1}), I - *attractive* ($\epsilon = 5.0$ kJ mol^{-1}), II - *almost attractive* ($\epsilon = 4.5$ kJ mol^{-1}), III - *semi attractive* ($\epsilon = 4.0$ kJ mol^{-1}), IV - *intermediate* ($\epsilon = 3.5$ kJ mol^{-1}), V - *almost intermediate* ($\epsilon = 3.1$ kJ mol^{-1}), VI - *semi repulsive* ($\epsilon = 2.7$ kJ mol^{-1}), VII - *almost repulsive* ($\epsilon = 2.3$ kJ mol^{-1}), VIII - *repulsive* ($\epsilon = 2.0$ kJ mol^{-1}), IX - *supra repulsive* ($\epsilon = 2.0$ kJ mol^{-1}). The value of σ is set to 0.47 nm for all levels of interactions except for level IX for which it is set to 0.62 nm.

Type	Q_d	Q_a	Q_0	Q_{SI}	P_4	N_d	N_{SN}	C_2
Q_d	I	0	II	II	0	III	0	IX
Q_a	0	I	II	II	0	I	II	IX
Q_0	II	II	IV	II	0	III	II	IX
Q_{SI}	II	II	II	0	II	III	0	IV
P_4	0	0	0	II	I	III	II	VII
N_d	III	I	III	III	III	III	0	VI
N_{SN}	0	II	II	0	II	0	0	IV
C_2	IX	IX	IX	IV	VII	VI	IV	IV

Simulations of HMS materials synthesis Large CG simulations used to investigate the synthesis of HMS materials at different pH conditions were performed in the *NPT* ensemble fixing temperature at 50 °C, pressure at 1 bar and following exactly the same simulation protocol used for the small CG systems used in the model development. Table S9 provides a list of all the simulations performed.

Table S9: Number of beads, simulation length and final box size for each coarse-grained MD simulation of HMS materials.

System	DDA^+	DDA	Cl^-	SI	SN	TMA^+	SISI	SISN	SNSN	water	time (ns)	box (nm)
DDA^+	1000		1000							61636	1200	20.1
DDA		1000								63136	600	20.1
DDA^+ + SI	1000			1000						63136	1200	20.2
DDA + SI		1000		1000		1000				63136	600	20.3
DDA + SN		1000			1000					63136	600	20.2
DDA^+ + SI + SN	1000		770	230	770					63136	2400	20.3
DDA^+ + DDA + SI + SN	890	110	660	230	770					63136	2400	20.3
DDA^+ + 1to1 SISN + SNSN	1000		880					120	380	61816	3000	20.2
DDA^+ + 2to1 SISN + SNSN	1000		760					240	760	61996	1800	20.3
DDA^+ + 3to1 SISN + SNSN	1000		640					360	1400	62176	600	20.4
DDA^+ + 4to1 SISN + SNSN	1000		520					480	1520	62356	1200	20.4

4 Additional results

The monomeric solution at pH $\sim$ 9.2 Figure S15 shows a comparison of the final snapshots obtained when simulating the monomeric solution at the measured pH of 9.2 (approximately corresponding to 23 % anionic silica monomers and 77 % neutral silica monomers) with 100 % charged DDA surfactants (Figure S15-a) and with respectively 89 % charged and 11 % neutral DDA surfactants (Figure S15-b).

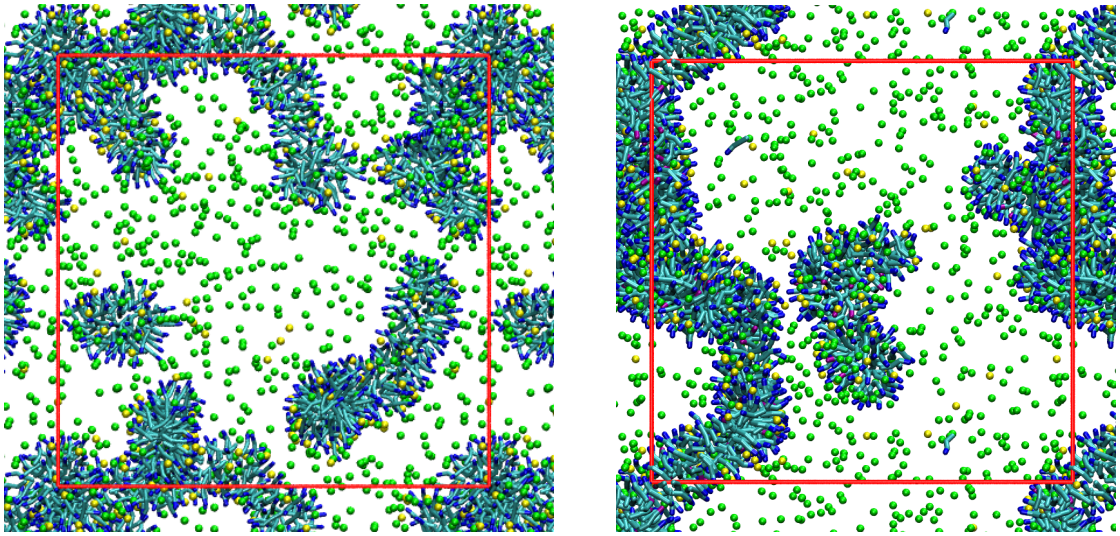

(a) (b)

Figure S15: Simulation snapshots obtained for aqueous DDA solutions at 0.22 M with 23 % anionic silica monomers and 77 % neutral silica monomers (pH $\sim$ 9.2): (a) with 100 % charged surfactants and (b) with 89 % charged and 11 % neutral surfactants. Water has been removed for clarity. Parts of the periodic images have been included to aid visualisation. Colour code is: charged heads, blue; neutral heads, purple; tails, teal; SI monomers, yellow; SN monomers, green.

Number of contacts To show that anionic silicates preferentially interact with surfactant head groups, we have calculated the number of contacts between surfactants and silicate species for the system containing charged surfactants and both charged (SI) and neutral (SN) silica monomers (see Figure 4a of the main document). This was done using the utility *g_ mindist* by fixing a cut-off distance of 0.97 nm and dividing the value obtained by the total number of SI or SN species in solution (i.e. 230 for SI and 770 for SN). Figure S16 shows that

during the simulation time an overwhelmingly larger number of contacts are formed between surfactant heads and anionic silica monomers, supporting the idea that SI monomers will strongly adsorb on DDA^+ micelles while SN-head contacts are residual.

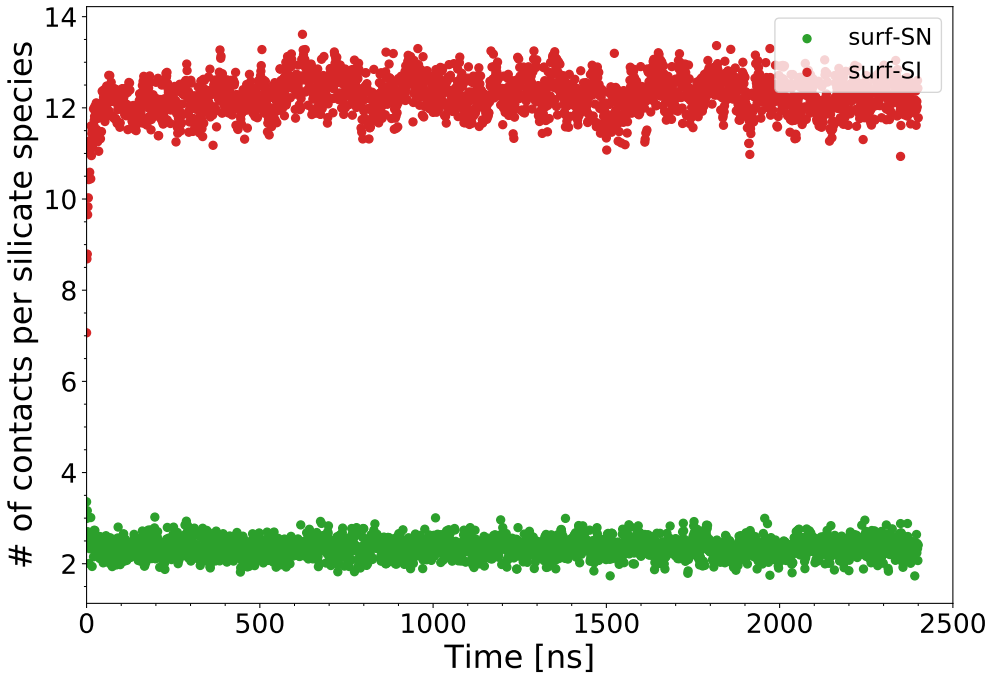

Figure S16: Number of contacts per silicate species obtained for the system containing charged surfactants and both SI and SN silica. Surfactants-SI, red and Surfactants-SN, green.

Hydrogen bond analysis To better understand the interactions occurring in the neutral system, formation of hydrogen bonds was assessed using the utility *g_hbond* based on AA simulations of silica/surfactant solutions. Indeed, hydrogen bonds are formed between neutral silica monomers and the neutral surfactant heads. However, calculation of the donor-acceptor distribution distances indicates that this interaction is quite weak compared to the other hydrogen bond interactions taking place in the system (see Figure S17).

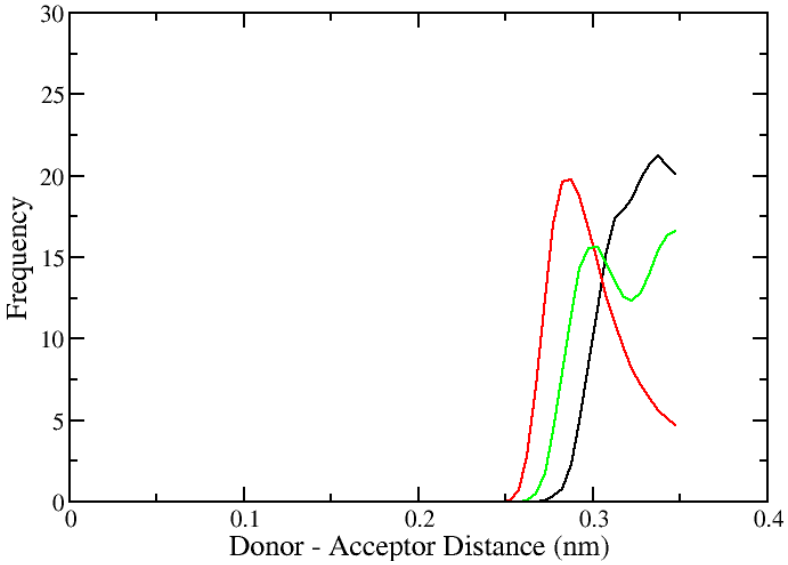

Figure S17: Distributions of donor-acceptor distances for the system containing a preformed micelle of DDA with SN monomers. Black, between surfactant heads and SN monomers; red, between surfactant heads and water; green, between SN monomers and water.

As described by Jeffrey, hydrogen bonds can be classified according to their donor-acceptor distance into "strong, mostly covalent" (between 0.22 and 0.25 nm), "moderate, mostly electrostatic" (between 0.25 and 0.32 nm) and "weak, electrostatic" (between 0.32 and 0.4 nm)[22]. Figure S17 shows that the donor-acceptor distance for the hydrogen bonds formed between surfactant heads and SN monomers (black line) is in the range of weak electrostatic interactions, whereas the hydrogen bonds formed by water with surfactant heads and SN monomers (red and green lines, respectively) correspond to moderate electrostatic interactions. As such, the affinity observed between SN and surfactants micelles is most likely due to hydrophobic interactions than to hydrogen bond formation in these systems.

References

(1) Tanev, P. T.; Pinnavaia, T. J. A Neutral Templating Route to Mesoporous Molecular Sieves. **1995**, *267*, 865–867.

(2) National Institute of Advanced Industrial Science and Technology Spectral database SDBS. 1999; `https://sdbs.db.aist.go.jp/sdbs/cgi-bin/landingpage?sdbsno=2391`, [Online accessed 05-September-2018].

(3) Berendsen, H. J. C.; Grigera, J. R.; Straatsma, T. P. The missing term in effective pair potentials. *The Journal of Physical Chemistry* **1987**, *91*, 6269–6271.

(4) Jorgensen, W. L.; Maxwell, D. S.; Tirado-Rives, J. Development and Testing of the OPLS All-Atom Force Field on Conformational Energetics and Properties of Organic Liquids. *Journal of the American Chemical Society* **1996**, *118*, 11225–11236.

(5) Wang, J.; Wolf, R. M.; Caldwell, J. W.; Kollman, P. A.; Case, D. A. Development and testing of a general amber force field. *Journal of Computational Chemistry* **2004**, *25*, 1157–1174.

(6) Jorge, M.; Gomes, J. R. B.; Cordeiro, M. N. D. S.; Seaton, N. A. Molecular Dynamics Simulation of the Early Stages of the Synthesis of Periodic Mesoporous Silica. *The Journal of Physical Chemistry B* **2009**, *113*, 708–718.

(7) Hess, B.; Bekker, H.; Berendsen, H. J. C.; Fraaije, J. G. E. M. LINCS: A linear constraint solver for molecular simulations. *Journal of Computational Chemistry* **1997**, *18*, 1463–1472.

(8) Darden, T.; York, D.; Pedersen, L. Particle mesh Ewald: An N log(N) method for Ewald sums in large systems. *The Journal of Chemical Physics* **1993**, *98*, 10089–10092.

(9) Darden, T.; Perera, L.; Li, L.; Pedersen, L. New tricks for modelers from the crystallog-

raphy toolkit: the particle mesh Ewald algorithm and its use in nucleic acid simulations. *Structure* **1999**, *7*, R55–R60.

(10) Martínez, L.; Andrade, R.; Birgin, E. G.; Martínez, J. M. PACKMOL: a package for building initial configurations for molecular dynamics simulations. *Journal of Computational Chemistry* **2009**, *30*, 2157–2164.

(11) Malliaris, A.; Le Moigne, J.; Sturm, J.; Zana, R. Temperature dependence of the micelle aggregation number and rate of intramicellar excimer formation in aqueous surfactant solutions. *The Journal of Physical Chemistry* **1985**, *89*, 2709–2713.

(12) Jorge, M.; Gomes, J. R. B.; Cordeiro, M. N. D. S.; Seaton, N. A. Molecular Simulation of Silica/Surfactant Self-Assembly in the Synthesis of Periodic Mesoporous Silicas. *Journal of the American Chemical Society* **2007**, *129*, 15414–15415.

(13) Jorge, M. Molecular Dynamics Simulation of Self-Assembly of n-Decyltrimethylammonium Bromide Micelles. *Langmuir* **2008**, *24*, 5714–5725.

(14) Nosé, S. A molecular dynamics method for simulations in the canonical ensemble. *Molecular Physics* **1984**, *52*, 255–268.

(15) Parrinello, M.; Rahman, A. Polymorphic transitions in single crystals: A new molecular dynamics method. *Journal of Applied Physics* **1981**, *52*, 7182–7190.

(16) Hockney, R.; Goel, S.; Eastwood, J. Quiet high-resolution computer models of a plasma. *Journal of Computational Physics* **1974**, *14*, 148–158.

(17) Marrink, S. J.; Risselada, H. J.; Yefimov, S.; Tieleman, D. P.; de Vries, A. H. The MARTINI Force Field: Coarse Grained Model for Biomolecular Simulations. *J. Phys. Chem. B* **2007**, *111*, 7812–7824.

(18) Pérez-Sánchez, G.; Chien, S.-C.; Gomes, J. R. B.; Cordeiro, M. N. D. S.; Auerbach, S. M.; Monson, P. A.; Jorge, M. Multiscale Model for the Templated Synthesis

of Mesoporous Silica: The Essential Role of Silica Oligomers. *Chemistry of Materials* **2016**,

(19) Bussi, G.; Donadio, D.; Parrinello, M. Canonical sampling through velocity rescaling. *The Journal of Chemical Physics* **2007**, *126*, 014101.

(20) Hoshen, J.; Kopelman, R. Percolation and cluster distribution. I. Cluster multiple labeling technique and critical concentration algorithm. *Physical Review B* **1976**, *14*, 3438–3445.

(21) CAMEO Chemicals, DODECANAMINE | CAMEO Chemicals | NOAA. `https://cameochemicals.noaa.gov/chemical/21833`, [Online accessed 13-March-2017].

(22) Jeffrey, G. *An Introduction to Hydrogen Bonding*; Topics in Physical Chemistry - Oxford University Press; Oxford University Press, 1997.